FEI3301: Homework 3

Balwan Rana and Brage Svendsen

January 26, 2024

Cylindrical resonance cavity excited with TEM and TM_{0n}-modes.

Cylindrical resonance cavity connected to aligned coaxial cables. Due to the azimuthal symmetry, only the TEM and TM_{0n} waveguide modes are excited. In terms of short-circuited cavity modes, only the TM_{0np}-modes are excited.

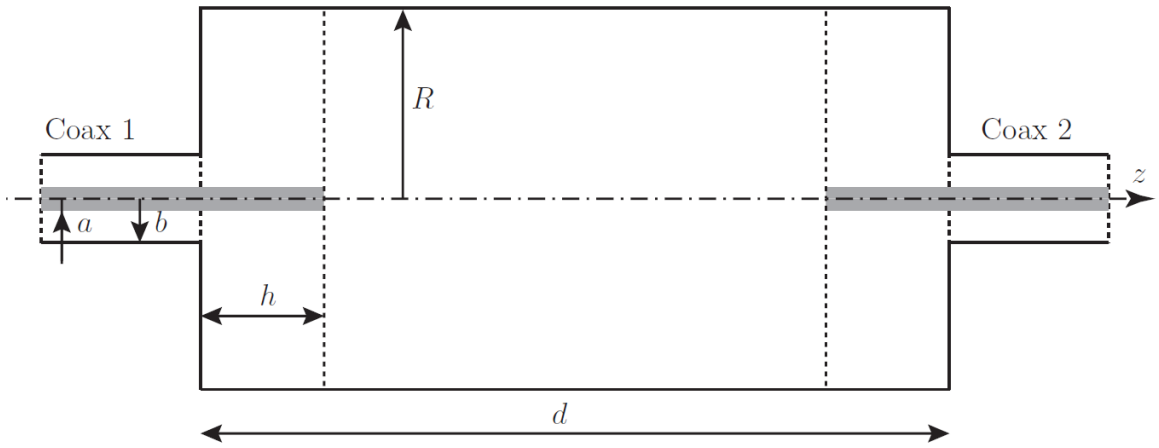

Figure 1: Cylindrical resonance cavity excited with TM_{0np}-modes.

Design parameters:

- Cavity radius (R) and length (d).
- Coaxial feeders: inner and outer radii (a, b); probe length (h) into the cavity.

Methodology:

- Mode-matching and cascading applied to five sections of waveguides.
- General-purpose software for comparison/verification.

Assignments:

1. Determine the 2×2 scattering matrix relating the dominant TEM-modes in the coaxial connectors.
2. Determine the observed resonance frequencies for the loaded cavity and compare them with the results for the unloaded cavity.
3. Determine the loaded Q-values at the resonance frequencies.
4. Determine the current distributions on the probes and compare them with the standing wave approximation.

1 Determine the 2×2 scattering matrix relating the dominant TEM-modes in the coaxial connectors.

The 2×2 scattering matrix relating the dominant TEM-modes in the coaxial connectors could be determined using the theory documented in Chapter 5.8 of the course compendium, sub-chapters 5.8.1 and 5.8.2. We will make use of the complete power normalized frequency domain electric and magnetic field expressions using Eq.A.22, Eq.A.23, Eq.A.28 and Eq.A.29 in Appendix A. Looking back to Figure 1, we assume that the wave propagation occurs to the right (from Coax 1 to Coax 2) and that A_1 and A_2 denote the first- and second-coming waveguide cross-sections where $A_1 \subset A_2$. We further assume that the cross-sectional junction between waveguide occurs at $z = z_0$, where we define the limits $z_1 = z_0 - 0$ and $z_2 = z_0 + 0$ for respective waveguide cross-section. The transversal TEM-mode fields are re-written from Eq.A.22, Eq.A.23, Eq.A.28 and Eq.A.29 in Appendix A as follows:

$$\left.\begin{aligned} \boldsymbol{E}_t(\mathbf{r}) &= \left[a_0^+(z) + a_0^-(z)\right] \boldsymbol{E}_{t0}(\boldsymbol{\rho}) \\ \boldsymbol{H}_t(\mathbf{r}) &= \left[a_0^+(z) - a_0^-(z)\right] \boldsymbol{H}_{t0}(\boldsymbol{\rho}) \end{aligned}\right\} \tag{1.1}$$

Here we have that $a_0^{\pm}(z) = a_0^{\mathrm{D}\pm} e^{\mp jkz}$ and $\{\boldsymbol{E}_{t0}(\boldsymbol{\rho}), \boldsymbol{E}_{t0}(\boldsymbol{\rho})\} = \{\boldsymbol{E}_0^{\mathrm{D}+}(\boldsymbol{\rho}), \boldsymbol{H}_0^{\mathrm{D}+}(\boldsymbol{\rho})\}$. Given that we are only working with TEM-modes in a junction between concentric coaxial waveguides, a coaxial connector, the expansion coefficient column vectors $\{\boldsymbol{a}^+(z), \boldsymbol{a}^-(z)\}$, the diagonal matrices $\mathbf{D}_1$ and $\mathbf{D}_2$, and the mode-coupling matrix $\mathbf{C}$ all become rank-0 tensors and could be obtained as follows:

$$\left.\begin{aligned} \boldsymbol{a}^+(z) &= a_0^+(z) \\ \boldsymbol{a}^-(z) &= a_0^-(z) \end{aligned}\right\} \tag{1.2}$$

$$\begin{aligned} D_{100} &= s_0^{(1)} \delta_{00} \\ &= \frac{1}{2} \int_{A_1} \left(\boldsymbol{E}_{t0}^{(1)} \times \boldsymbol{H}_{t0}^{(1)*} \right) \cdot \hat{\mathbf{z}} ds \\ &= \frac{1}{2} \int_0^{2\pi} \int_{r_{i,1}}^{r_{o,1}} \left(\boldsymbol{E}_{t0}^{(1)} \times \boldsymbol{H}_{t0}^{(1)*} \right) \cdot \hat{\mathbf{z}} \rho d\rho d\varphi \\ &= \frac{1}{2} \int_0^{2\pi} \int_{r_{i,1}}^{r_{o,1}} \left(\frac{1}{\pi} \ln\left(\frac{r_{o,1}}{r_{i,1}} \right)^{-1} \frac{1}{\rho^2} \right) \rho d\rho d\varphi \\ &= 1 \end{aligned} \tag{1.3}$$

$$\begin{aligned} D_{200} &= s_0^{(2)} \delta_{00} \\ &= \frac{1}{2} \int_{A_2} \left(\boldsymbol{E}_{t0}^{(2)} \times \boldsymbol{H}_{t0}^{(2)*} \right) \cdot \hat{\mathbf{z}} ds \\ &= \frac{1}{2} \int_0^{2\pi} \int_{r_{i,2}}^{r_{o,2}} \left(\boldsymbol{E}_{t0}^{(2)} \times \boldsymbol{H}_{t0}^{(2)*} \right) \cdot \hat{\mathbf{z}} \rho d\rho d\varphi \\ &= \frac{1}{2} \int_0^{2\pi} \int_{r_{i,2}}^{r_{o,2}} \left(\frac{1}{\pi} \ln\left(\frac{r_{o,2}}{r_{i,2}} \right)^{-1} \frac{1}{\rho^2} \right) \rho d\rho d\varphi \\ &= 1 \end{aligned} \tag{1.4}$$

$$
\begin{aligned}
C_{00} &= \frac{1}{2}\int_{A_1}\left(\boldsymbol{E}_{t0}^{(1)}\times\boldsymbol{H}_{t0}^{(2)*}\right)\cdot\hat{\mathbf{z}}ds \\
&= \frac{1}{2}\int_0^{2\pi}\int_{r_{i,1}}^{r_{o,1}}\left(\boldsymbol{E}_{t0}^{(1)}\times\boldsymbol{H}_{t0}^{(2)*}\right)\cdot\hat{\mathbf{z}}\rho d\rho d\varphi \\
&= \frac{1}{2}\int_0^{2\pi}\int_{r_{i,1}}^{r_{o,1}}\left(\frac{1}{\pi}\sqrt{\ln\left(\frac{r_{o,1}}{r_{i,1}}\right)^{-1}\ln\left(\frac{r_{o,2}}{r_{i,2}}\right)^{-1}}\frac{1}{\rho^2}\right)\rho d\rho d\varphi \\
&= \sqrt{\frac{\ln\left(\frac{r_{o,1}}{r_{i,1}}\right)}{\ln\left(\frac{r_{o,2}}{r_{i,2}}\right)}}
\end{aligned}
\tag{1.5}
$$

Here we have that $\{r_{i,1}, r_{o,1}\}$ and $\{r_{i,2}, r_{o,2}\}$ represent the inner and outer circular coaxial radius for the first- and second-coming waveguide cross-section. Using the tensor formulation of the aforementioned quantities, we could construct a linear equation system in order to obtain the scattering matrix relating the dominant TEM-modes in the coaxial connectors:

$$
\left.
\begin{aligned}
\mathbf{D}_2\left[\boldsymbol{a}^+(z_2)+\boldsymbol{a}^-(z_2)\right] &= \mathbf{C}^T\left[\boldsymbol{a}^+(z_1)+\boldsymbol{a}^-(z_1)\right] \\
\mathbf{D}_1^*\left[\boldsymbol{a}^+(z_1)-\boldsymbol{a}^-(z_1)\right] &= \mathbf{C}^*\left[\boldsymbol{a}^+(z_2)-\boldsymbol{a}^-(z_2)\right]
\end{aligned}
\right\}
\tag{1.6}
$$

$$
\begin{bmatrix}\boldsymbol{a}^-(z_1)\\ \boldsymbol{a}^+(z_2)\end{bmatrix} = \begin{bmatrix}\mathbf{S}_{11} & \mathbf{S}_{12}\\ \mathbf{S}_{21} & \mathbf{S}_{22}\end{bmatrix}\begin{bmatrix}\boldsymbol{a}^+(z_1)\\ \boldsymbol{a}^-(z_2)\end{bmatrix}
\tag{1.7}
$$

Here the superscript T and * represent the transpose and the conjugate of a tensor respectively. The scattering coefficients $\mathbf{S}_{mn}$ for the dominant TEM-modes in the coaxial connectors are defined as follows:

$$
\begin{aligned}
\mathbf{S}_{11} &= \left(\mathbf{D}_1^* + \mathbf{C}^*\mathbf{D}_2^{-1}\mathbf{C}^T\right)^{-1}\left(\mathbf{D}_1^* - \mathbf{C}^*\mathbf{D}_2^{-1}\mathbf{C}^T\right) \\
&= \left(1+\frac{\ln\left(\frac{r_{o,1}}{r_{i,1}}\right)}{\ln\left(\frac{r_{o,2}}{r_{i,2}}\right)}\right)^{-1}\left(1-\frac{\ln\left(\frac{r_{o,1}}{r_{i,1}}\right)}{\ln\left(\frac{r_{o,2}}{r_{i,2}}\right)}\right) \\
&= \frac{\ln\left(\frac{r_{o,2}}{r_{i,2}}\right)-\ln\left(\frac{r_{o,1}}{r_{i,1}}\right)}{\ln\left(\frac{r_{o,2}}{r_{i,2}}\right)+\ln\left(\frac{r_{o,1}}{r_{i,1}}\right)}
\end{aligned}
\tag{1.8}
$$

$$
\begin{aligned}
\mathbf{S}_{12} &= 2\left(\mathbf{D}_1^* + \mathbf{C}^*\mathbf{D}_2^{-1}\mathbf{C}^T\right)^{-1}\mathbf{C}^* \\
&= 2\left(1+\frac{\ln\left(\frac{r_{o,1}}{r_{i,1}}\right)}{\ln\left(\frac{r_{o,2}}{r_{i,2}}\right)}\right)^{-1}\sqrt{\frac{\ln\left(\frac{r_{o,1}}{r_{i,1}}\right)}{\ln\left(\frac{r_{o,2}}{r_{i,2}}\right)}} \\
&= \frac{2\ln\left(\frac{r_{o,2}}{r_{i,2}}\right)}{\ln\left(\frac{r_{o,2}}{r_{i,2}}\right)+\ln\left(\frac{r_{o,1}}{r_{i,1}}\right)}\sqrt{\frac{\ln\left(\frac{r_{o,1}}{r_{i,1}}\right)}{\ln\left(\frac{r_{o,2}}{r_{i,2}}\right)}}
\end{aligned}
\tag{1.9}
$$

$$
\begin{aligned}
\mathbf{S}_{21} &= 2\left(\mathbf{C}^T\left(\mathbf{D}_1^*\right)^{-1}\mathbf{C}^* + \mathbf{D}_2\right)^{-1}\mathbf{C}^T \\
&= 2\left(\frac{\ln\left(\frac{r_{o,1}}{r_{i,1}}\right)}{\ln\left(\frac{r_{o,2}}{r_{i,2}}\right)} + 1\right)^{-1}\sqrt{\frac{\ln\left(\frac{r_{o,1}}{r_{i,1}}\right)}{\ln\left(\frac{r_{o,2}}{r_{i,2}}\right)}} \\
&= \frac{2\ln\left(\frac{r_{o,2}}{r_{i,2}}\right)}{\ln\left(\frac{r_{o,2}}{r_{i,2}}\right) + \ln\left(\frac{r_{o,1}}{r_{i,1}}\right)}\sqrt{\frac{\ln\left(\frac{r_{o,1}}{r_{i,1}}\right)}{\ln\left(\frac{r_{o,2}}{r_{i,2}}\right)}}
\end{aligned}
\tag{1.10}
$$

$$
\begin{aligned}
\mathbf{S}_{22} &= \left(\mathbf{C}^T\left(\mathbf{D}_1^*\right)^{-1}\mathbf{C}^* + \mathbf{D}_2\right)^{-1}\left(\mathbf{C}^T\left(\mathbf{D}_1^*\right)^{-1}\mathbf{C}^* - \mathbf{D}_2\right) \\
&= \left(\frac{\ln\left(\frac{r_{o,1}}{r_{i,1}}\right)}{\ln\left(\frac{r_{o,2}}{r_{i,2}}\right)} + 1\right)^{-1}\left(\frac{\ln\left(\frac{r_{o,1}}{r_{i,1}}\right)}{\ln\left(\frac{r_{o,2}}{r_{i,2}}\right)} - 1\right) \\
&= \frac{\ln\left(\frac{r_{o,1}}{r_{i,1}}\right) - \ln\left(\frac{r_{o,2}}{r_{i,2}}\right)}{\ln\left(\frac{r_{o,2}}{r_{i,2}}\right) + \ln\left(\frac{r_{o,1}}{r_{i,1}}\right)}
\end{aligned}
\tag{1.11}
$$

If we instead assumed that the wave propagation occurs to the left (from Coax 2 to Coax 1), then $A_2 \subset A_1$ given that we are using the same naming convention introduced in the aforementioned text. This change would result in a swap between the media indices in the mode-coupling matrix $\mathbf{C}$, which in turn would alter the expressions for the scattering coefficients $\mathbf{S}_{mn}$. However, since the change itself and the related expressions are trivial, we refrain from re-writing the scattering coefficients $\mathbf{S}_{mn}$ and the mode-coupling matrix $\mathbf{C}$ for this case.

2 Determine the observed resonance frequencies for the loaded cavity and compare them with the results for the unloaded cavity.

For an unloaded cavity, the resonance frequencies for the TM_{0np}-modes are determined in Chapter 6, sub-chapter 6.1, in the Compendium and could be defined as follows:

$$\begin{aligned} f_{0np} &= \frac{c_0 k_{0np}}{2\pi} \\ &= \frac{1}{2\sqrt{\varepsilon_0\mu_0}}\sqrt{\left(\frac{k_{t0n}}{\pi}\right)^2 + \left(\frac{p}{d}\right)^2} \\ &= \frac{1}{2\sqrt{\varepsilon_0\mu_0}}\sqrt{\left(\frac{d_{t0n}}{\pi}\right)^2 + \left(\frac{p}{d}\right)^2} \\ &= \frac{1}{2\sqrt{\varepsilon_0\mu_0}}\sqrt{\left(\frac{\xi_{0n}}{\pi r_o}\right)^2 + \left(\frac{p}{d}\right)^2} \end{aligned} \tag{2.1}$$

Here we have that $\{c_0, \varepsilon_0, \mu_0\}$ are the speed of light, the permittivity, and the permeability in free-space respectively. In addition, ξ_{mn} is the nth zero of the zeroth order Bessel function of the first kind, r_0 is the cavity radius, k_{mnp} is the cavity wave number, d is the cavity length, and p is the longitudinal mode variation where $p \subset \mathbb{Z}^+$. From Appendix B and C, we know that $m \subset \mathbb{Z}^+$ and $n \subset \mathbb{N}$.

For a loaded cavity, the resonance frequencies are observed using the loaded scattering matrix. The loaded scattering matrix is determined using cascading of the scattering and propagation matrices between each waveguide cross-section. Looking back to Figure 1, we assume that the wave propagation occurs to the right (from Coax 1 to Coax 2) and that $\boldsymbol{A_1}$ and $\boldsymbol{A_2}$ denote the first- and second-coming waveguide cross-sections. We further assume that the cross-sectional junction between waveguide occurs at $z = z_0$, where we define the limits $z_1 = z_0 - 0$ and $z_2 = z_0 + 0$ for respective waveguide cross-section. For the cross-sectional junction between waveguide geometries, the transversal modal fields from Appendix B and C are re-written as follows:

$$\boldsymbol{E}_t(\mathbf{r}) = \sum_{i=1} \left[a_i^+(z) + a_i^-(z)\right] \boldsymbol{E}_{ti}(\boldsymbol{\rho}) \tag{2.2}$$

$$\boldsymbol{H}_t(\mathbf{r}) = \sum_{i=1} \left[a_i^+(z) - a_i^-(z)\right] \boldsymbol{H}_{ti}(\boldsymbol{\rho}) \tag{2.3}$$

Here we have that $\left\{a_i^{\pm}(z) = a_i^{\mathrm{D}\pm} e^{\mp j d_{zi} z}\right\}$ and $\{\boldsymbol{E}_{ti}(\boldsymbol{\rho}), \boldsymbol{H}_{ti}(\boldsymbol{\rho})\} = \left\{\boldsymbol{E}_{ti}^{\mathrm{D}}(\boldsymbol{\rho}), \boldsymbol{H}_{ti}^{\mathrm{D}}(\boldsymbol{\rho})\right\}$, where we emphasize the fact that only the transversal modal field components are considered. In addition, we have denoted $\{i = mn\}$ as a collective term for representing the TM_{mn} modes, which is introduced for convenience. For the cross-sectional junction between two unique waveguide geometries, we have two separate cases of geometrical considerations: (1) $\{\boldsymbol{A_1} \subset \boldsymbol{A_2}\}$ and (2) $\{\boldsymbol{A_2} \subset \boldsymbol{A_1}\}$. For case (1) $\{\boldsymbol{A_1} \subset \boldsymbol{A_2}\}$, we get the following tangential boundary conditions for the transversal modal fields:

$$\boldsymbol{E}_t(\boldsymbol{\rho}, z_2) = \begin{cases} \mathbf{0}, & \boldsymbol{\rho} \in \boldsymbol{A_2} - \boldsymbol{A_1} \\ \boldsymbol{E}_t(\boldsymbol{\rho}, z_1), & \boldsymbol{\rho} \in \boldsymbol{A_1} \end{cases} \tag{2.4}$$

$$\boldsymbol{H}_t(\boldsymbol{\rho}, z_1) = \boldsymbol{H}_t(\boldsymbol{\rho}, z_2), \quad \boldsymbol{\rho} \in \boldsymbol{A_1} \tag{2.5}$$

For case (2) $\{\boldsymbol{A_2} \subset \boldsymbol{A_1}\}$, we get the following tangential boundary conditions for the transversal modal fields:

$$\boldsymbol{E}_t(\boldsymbol{\rho}, z_1) = \begin{cases} \mathbf{0}, & \boldsymbol{\rho} \in \boldsymbol{A_1} - \boldsymbol{A_2} \\ \boldsymbol{E}_t(\boldsymbol{\rho}, z_2), & \boldsymbol{\rho} \in \boldsymbol{A_2} \end{cases} \tag{2.6}$$

$$\boldsymbol{H}_t(\boldsymbol{\rho}, z_1) = \boldsymbol{H}_t(\boldsymbol{\rho}, z_2), \quad \boldsymbol{\rho} \in \boldsymbol{A_2} \tag{2.7}$$

Moving forward, we will denote $\{i = 0n\}$ and $\{j = 0q\}$ as collective terms for representing two independent $\mathrm{TM}_{0\{x=n,q\}}$ modes. The sub- and superscripts $\{1, 2\}$ represent a reference to the first- or second-coming waveguide geometry and their associated modal fields and properties. In order to obtain the loaded scattering matrix, we first have to calculate the expansion coefficient column vectors $\{\boldsymbol{a}^+(z), \boldsymbol{a}^-(z)\}$, diagonal matrices $\{\mathbf{D}_1, \mathbf{D}_2\}$, and the mode-coupling matrix $\mathbf{C}$ whilst considering the different tangential boundary conditions and cross-sectional waveguide junctions. The expansion coefficient column vectors $\{\boldsymbol{a}^+(z), \boldsymbol{a}^-(z)\}$ are independent of the cross-sectional waveguide geometry and the tangential boundary conditions. The expansion coefficient column vectors $\{\boldsymbol{a}^+(z), \boldsymbol{a}^-(z)\}$ could be expressed as follows:

$$\begin{aligned} \boldsymbol{a}^+(z) &= \sum_{i=1} a_i^+(z) \\ &= \sum_{n=1} a_{0n}^+(z) \\ &= \sum_{n=1} a_{0n}^{\mathrm{D}+} e^{-jd_{z0n}z} \end{aligned} \tag{2.8}$$

$$\begin{aligned} \boldsymbol{a}^-(z) &= \sum_{i=1} a_i^-(z) \\ &= \sum_{n=1} a_{0n}^-(z) \\ &= \sum_{n=1} a_{0n}^{\mathrm{D}-} e^{+jd_{z0n}z} \end{aligned} \tag{2.9}$$

The general diagonal matrix $\{\mathbf{D}_N\}$ is dependent on the cross-sectional waveguide geometry, but not on the tangential boundary conditions. The general diagonal matrix $\{\mathbf{D}_N\}$ could be expressed as follows:

$$\begin{aligned} D_{Nij} &= s_i^{(N)} \delta_{ij} \\ &= s_{m=0,n}^{(N)} \delta_{mp} \delta_{nq} \\ &= \frac{1}{2} \int_{A_N} \left(\boldsymbol{E}_{t0n}^{(N)} \times \boldsymbol{H}_{t0q}^{(N)*} \right) \cdot \hat{\mathbf{z}} ds \\ &= \frac{1}{2} \int_{A_N} \left(\boldsymbol{E}_{t0n}^{\mathrm{D}(N)}(\boldsymbol{\rho}) \times \boldsymbol{H}_{t0q}^{\mathrm{D}(N)*}(\boldsymbol{\rho}) \right) \cdot \hat{\mathbf{z}} ds \\ &= \frac{1}{2} \int_{A_N} \left(\boldsymbol{e}_{0n}^{\mathrm{D}(N)}(\boldsymbol{\rho}) \times \frac{k}{\eta d_{z0q,N}^*} \boldsymbol{h}_{0q}^{\mathrm{D}(N)}(\boldsymbol{\rho}) \right) \cdot \hat{\mathbf{z}} ds \\ &= \frac{1}{2} \frac{k}{\eta d_{z0q,N}^*} \int_{A_N} \left(\boldsymbol{e}_{0n}^{\mathrm{D}(N)}(\boldsymbol{\rho}) \times \boldsymbol{h}_{0q}^{\mathrm{D}(N)}(\boldsymbol{\rho}) \right) \cdot \hat{\mathbf{z}} ds \\ &= \frac{1}{2} \frac{k}{\eta d_{z0q,N}^*} d_{t0n,N}^2 D_{0n,N}^2 \delta_{nq} \\ &= \frac{|d_{z0n,N}|}{d_{z0q,N}^*} \delta_{nq} \\ &= \frac{d_{z0n,N}}{|d_{z0n,N}|} \delta_{nq} \\ &= \frac{\sqrt{k^2 - d_{t0n,N}^2}}{\left| \sqrt{k^2 - d_{t0n,N}^2} \right|} \delta_{nq} \end{aligned} \tag{2.10}$$

Here we have made use of the transversal modal field's inherited orthogonality relation from the eigenfunctions, which is defined in Eq.5.67a in the Compendium for the Dirichlet eigenvalue problem. We also acknowledge that if the longitudinal eigenvalue d_{zi}^* is real-valued, assuming we are only considering propagating modes and no evanescent modes, then $\{\mathbf{D}_1, \mathbf{D}_2\} = 1$ for power normalized modes. In addition, we acknowledge that the longitudinal eigenvalue for the TEM-mode is simply the wavenumber k since for these modes the transversal eigenvalue $d_{ti} = 0$. The diagonal matrix elements D_{00} for

TEM modes are defined in Section 1 above. In the last steps of Eq.1.3, we made use of the relationship $\{|x| = \sqrt{xx^*}\}$ for complex/imaginary-valued components and introduced the general expression for the longitudinal eigenvalue. Notice that the transversal eigenvalue depends on the cross-sectional waveguide geometry in question.

In the following subsections 2.1-2.4, we present the mode-coupling matrix $\mathbf{C}$ calculations for four separate cases. These cases involve the choice between: (1) $\{\boldsymbol{A_1} \subset \boldsymbol{A_2}\}$ and (2) $\{\boldsymbol{A_2} \subset \boldsymbol{A_1}\}$ of the tangential boundary conditions in two different cross-sectional junctions between waveguide geometries; and: (A) TM-TM and (B) TEM-TM modal field coupling. The case for the TEM-TEM modal field coupling at a junction between two circular coaxial waveguides with different outer radii has already been treated in Section 1. There are of course additional cases to consider if one wants to derive a complete description of the coupling between modal fields in two different geometries, however, we limit ourselves to the cases that are relevant to the assignment in question. Subsection 2.1 focuses on the TM-TM modal field coupling at a junction between two circular coaxial waveguides with different outer radii, and Subsection 2.2 focuses on the TEM-TM modal field coupling at the same junction. Furthermore, Subsection 2.3 focuses on the TM-TM modal field coupling at a junction between a circular coaxial waveguide and a circular waveguide (without an inner conductor) of the same outer radii, and Subsection 2.4 focuses on the TEM-TM modal field coupling at the same junction.

2.1 TM-TM modal field coupling at a junction between two circular coaxial waveguides with different outer radii.

In subsection 2.1, we make use of equations and properties derived in Appendix C. For case (1) $\{\boldsymbol{A_1} \subset \boldsymbol{A_2}\}$ of the aforementioned tangential boundary conditions, where we propagate from a coaxial circular waveguide with a smaller to a larger outer radius, we obtain the following result for the

mode-coupling matrix $\mathbf{C}$:

$$
\begin{aligned}
C_{ij} &= \frac{1}{2}\int_{A_1}\left(\boldsymbol{E}_{ti}^{(1)}\times\boldsymbol{H}_{tj}^{(2)*}\right)\cdot\hat{\mathbf{z}}ds \\
&= \frac{1}{2}\int_{A_1}\left(\boldsymbol{E}_{t0n}^{(1)}\times\boldsymbol{H}_{t0q}^{(2)*}\right)\cdot\hat{\mathbf{z}}ds \\
&= \frac{1}{2}\int_{A_1}\left(\boldsymbol{E}_{t0n}^{\mathrm{D}(1)}(\boldsymbol{\rho})\times\boldsymbol{H}_{t0q}^{\mathrm{D}(2)*}(\boldsymbol{\rho})\right)\cdot\hat{\mathbf{z}}ds \\
&= \frac{1}{2}\int_{A_1}\left(\boldsymbol{e}_{0n}^{\mathrm{D}(1)}(\boldsymbol{\rho})\times\frac{k}{\eta d_{z0q,2}^{*}}\boldsymbol{h}_{0q}^{\mathrm{D}(2)}(\boldsymbol{\rho})\right)\cdot\hat{\mathbf{z}}ds \\
&= \frac{\xi_{0n,1}\xi_{0q,2}}{\pi r_i^2 d_{t0n,1}d_{t0q,2}d_{z0q,2}^{*}}\sqrt{\frac{|d_{z0n,1}|\,|d_{z0q,2}|}{\left[r_i^2L_{-1}\left(\xi_{0n,1}\right)L_1\left(\xi_{0n,1}\right)-r_{o,1}^2L_{-1}\left(\xi_{0n,1}\frac{r_{o,1}}{r_i}\right)L_1\left(\xi_{0n,1}\frac{r_{o,1}}{r_i}\right)\right]}} \\
&\quad\times\frac{\displaystyle\int_0^{2\pi}\int_{r_i}^{r_{o,1}}\rho L_1\left(\xi_{0n,1}\frac{\rho}{r_i}\right)L_1\left(\xi_{0q,2}\frac{\rho}{r_i}\right)d\rho d\varphi}{\sqrt{\left[r_i^2L_{-1}\left(\xi_{0q,2}\right)L_1\left(\xi_{0q,2}\right)-r_{o,2}^2L_{-1}\left(\xi_{0q,2}\frac{r_{o,2}}{r_i}\right)L_1\left(\xi_{0q,2}\frac{r_{o,2}}{r_i}\right)\right]}} \\
&= \frac{2\xi_{0n,1}\xi_{0q,2}}{r_i^2 d_{t0n,1}d_{t0q,2}d_{z0q,2}^{*}}\sqrt{\frac{|d_{z0n,1}|\,|d_{z0q,2}|}{\left[r_{o,1}^2L_1\left(\xi_{0n,1}\frac{r_{o,1}}{r_i}\right)L_1\left(\xi_{0n,1}\frac{r_{o,1}}{r_i}\right)-r_i^2L_1\left(\xi_{0n,1}\right)L_1\left(\xi_{0n,1}\right)\right]}} \\
&\quad\times\frac{1}{\sqrt{\left[r_{o,2}^2L_1\left(\xi_{0q,2}\frac{r_{o,2}}{r_i}\right)L_1\left(\xi_{0q,2}\frac{r_{o,2}}{r_i}\right)-r_i^2L_1\left(\xi_{0q,2}\right)L_1\left(\xi_{0q,2}\right)\right]}} \\
&\quad\times\left[\frac{\xi_{0n,1}\frac{\rho}{r_i}L_2\left(\xi_{0n,1}\frac{\rho}{r_i}\right)L_1\left(\xi_{0q,2}\frac{\rho}{r_i}\right)-\xi_{0q,2}\frac{\rho}{r_i}L_1\left(\xi_{0n,1}\frac{\rho}{r_i}\right)L_2\left(\xi_{0q,2}\frac{\rho}{r_i}\right)}{\frac{\xi_{0n,1}^2-\xi_{0q,2}^2}{r_i^2}}\right]_{r_i}^{r_{o,1}}
\end{aligned}
\tag{2.11}
$$

Here we have made use of the relationship $\left\{|x|=\sqrt{xx^*}\right\}$ for complex/imaginary-valued components, the relationship $\left\{L_{-k}\left(x\right)=\left(-1\right)^kL_k\left(x\right)\right\}$, along with the following integral relation for the superposition of the first and second kind Bessel functions:

$$
\int xL_k\left(\alpha x\right)L_k\left(\beta x\right)dx=\frac{\alpha xL_{k+1}\left(\alpha x\right)L_k\left(\beta x\right)-\beta xL_k\left(\alpha x\right)L_{k+1}\left(\beta x\right)}{\alpha^2-\beta^2} \tag{2.12}
$$

The quantities $\{r_{o,1},r_{o,2}\}$ represent the outer circular coaxial radius for the first- and second-coming waveguide cross-section, whilst $\{r_i\}$ represents the common inner circular coaxial radius between the two waveguide geometries. In addition, the superscript $\{*\}$ represents the complex conjugation operator.

For case (2) $\{\boldsymbol{A_2}\subset\boldsymbol{A_1}\}$ of the aforementioned tangential boundary conditions, where we propagate from a coaxial circular waveguide with a larger to a smaller outer radius, we obtain the following result

for the mode-coupling matrix $\mathbf{C}$:

$$
\begin{aligned}
C_{ij} &= \frac{1}{2}\int_{A_2}\left(\boldsymbol{E}_{ti}^{(1)}\times\boldsymbol{H}_{tj}^{(2)*}\right)\cdot\hat{\mathbf{z}}ds \\
&= \frac{1}{2}\int_{A_2}\left(\boldsymbol{E}_{t0n}^{(1)}\times\boldsymbol{H}_{t0q}^{(2)*}\right)\cdot\hat{\mathbf{z}}ds \\
&= \frac{1}{2}\int_{A_2}\left(\boldsymbol{E}_{t0n}^{\mathrm{D}(1)}(\boldsymbol{\rho})\times\boldsymbol{H}_{t0q}^{\mathrm{D}(2)*}(\boldsymbol{\rho})\right)\cdot\hat{\mathbf{z}}ds \\
&= \frac{1}{2}\int_{A_2}\left(\boldsymbol{e}_{0n}^{\mathrm{D}(1)}(\boldsymbol{\rho})\times\frac{k}{\eta d_{z0q,2}^{*}}\boldsymbol{h}_{0q}^{\mathrm{D}(2)}(\boldsymbol{\rho})\right)\cdot\hat{\mathbf{z}}ds \\
&= \frac{\xi_{0n,1}\xi_{0q,2}}{\pi r_i^2 d_{t0n,1}d_{t0q,2}d_{z0q,2}^{*}}\sqrt{\frac{|d_{z0n,1}|\,|d_{z0q,2}|}{\left[r_i^2 L_{-1}\left(\xi_{0n,1}\right)L_1\left(\xi_{0n,1}\right)-r_{o,1}^2 L_{-1}\left(\xi_{0n,1}\frac{r_{o,1}}{r_i}\right)L_1\left(\xi_{0n,1}\frac{r_{o,1}}{r_i}\right)\right]}} \\
&\quad\times\frac{\displaystyle\int_0^{2\pi}\int_{r_i}^{r_{o,2}}\rho L_1\left(\xi_{0n,1}\frac{\rho}{r_i}\right)L_1\left(\xi_{0q,2}\frac{\rho}{r_i}\right)d\rho d\varphi}{\sqrt{\left[r_i^2 L_{-1}\left(\xi_{0q,2}\right)L_1\left(\xi_{0q,2}\right)-r_{o,2}^2 L_{-1}\left(\xi_{0q,2}\frac{r_{o,2}}{r_i}\right)L_1\left(\xi_{0q,2}\frac{r_{o,2}}{r_i}\right)\right]}} \\
&= \frac{2\xi_{0n,1}\xi_{0q,2}}{r_i^2 d_{t0n,1}d_{t0q,2}d_{z0q,2}^{*}}\sqrt{\frac{|d_{z0n,1}|\,|d_{z0q,2}|}{\left[r_{o,1}^2 L_1\left(\xi_{0n,1}\frac{r_{o,1}}{r_i}\right)L_1\left(\xi_{0n,1}\frac{r_{o,1}}{r_i}\right)-r_i^2 L_1\left(\xi_{0n,1}\right)L_1\left(\xi_{0n,1}\right)\right]}} \\
&\quad\times\frac{1}{\sqrt{\left[r_{o,2}^2 L_1\left(\xi_{0q,2}\frac{r_{o,2}}{r_i}\right)L_1\left(\xi_{0q,2}\frac{r_{o,2}}{r_i}\right)-r_i^2 L_1\left(\xi_{0q,2}\right)L_1\left(\xi_{0q,2}\right)\right]}} \\
&\quad\times\left[\frac{\xi_{0n,1}\frac{\rho}{r_i}L_2\left(\xi_{0n,1}\frac{\rho}{r_i}\right)L_1\left(\xi_{0q,2}\frac{\rho}{r_i}\right)-\xi_{0q,2}\frac{\rho}{r_i}L_1\left(\xi_{0n,1}\frac{\rho}{r_i}\right)L_2\left(\xi_{0q,2}\frac{\rho}{r_i}\right)}{\frac{\xi_{0n,1}^2-\xi_{0q,2}^2}{r_i^2}}\right]_{r_i}^{r_{o,2}}
\end{aligned}
\tag{2.13}
$$

Here we have made use of the same properties as for the aforementioned case. Note that the only difference with the mode-coupling matrix $\mathbf{C}$ between the two cases (1) $\{\boldsymbol{A_1}\subset\boldsymbol{A_2}\}$ and (2) $\{\boldsymbol{A_2}\subset\boldsymbol{A_1}\}$ is the integration cross-section and limits, along with the arguments between the functions $L_k\left(\alpha x\right)$ and $L_k\left(\beta x\right)$.

2.2 TEM-TM modal field coupling at a junction between two circular coaxial waveguides with different outer radii.

In subsection 2.2, we make use of equations and properties derived in Appendix A and C. For case (1) $\{\boldsymbol{A_1}\subset\boldsymbol{A_2}\}$ of the aforementioned tangential boundary conditions, where we propagate from a coaxial circular waveguide with a smaller to a larger outer radius, we obtain the following result for

the mode-coupling matrix $\mathbf{C}$:

$$
\begin{aligned}
C_{ij} &= \frac{1}{2}\int_{A_1}\left(\boldsymbol{E}_{ti}^{(1)}\times\boldsymbol{H}_{tj}^{(2)*}\right)\cdot\hat{\mathbf{z}}ds \\
&= \frac{1}{2}\int_{A_1}\left(\boldsymbol{E}_{t00}^{(1)}\times\boldsymbol{H}_{t0q}^{(2)*}\right)\cdot\hat{\mathbf{z}}ds \\
&= \frac{1}{2}\int_{A_1}\left(\boldsymbol{E}_{t00}^{\mathrm{D}(1)}(\boldsymbol{\rho})\times\boldsymbol{H}_{t0q}^{\mathrm{D}(2)*}(\boldsymbol{\rho})\right)\cdot\hat{\mathbf{z}}ds \\
&= \frac{1}{2}\int_{A_1}\left(\frac{1}{D_0}\boldsymbol{e}_{00}^{\mathrm{D}(1)}(\boldsymbol{\rho})\times\frac{k}{\eta d_{z0q,2}^{*}}\boldsymbol{h}_{0q}^{\mathrm{D}(2)}(\boldsymbol{\rho})\right)\cdot\hat{\mathbf{z}}ds \\
&= \mp\frac{\xi_{0q,2}}{2\pi r_i d_{t0q,2}d_{z0q,2}^{*}}\sqrt{\frac{2k\left|d_{z0q,2}\right|}{\ln\left(\frac{r_o}{r_i}\right)}}\frac{\displaystyle\int_0^{2\pi}\int_{r_i}^{r_{o,1}}L_1\left(\xi_{0q,2}\frac{\rho}{r_i}\right)d\rho d\varphi}{\sqrt{\left[r_i^2L_1\left(\xi_{0q,2}\right)L_1\left(\xi_{0q,2}\right)-r_o^2L_1\left(\xi_{0q,2}\frac{r_o}{r_i}\right)L_1\left(\xi_{0q,2}\frac{r_o}{r_i}\right)\right]}} \\
&= \mp\frac{\xi_{0q,2}}{r_i d_{t0q,2}d_{z0q,2}^{*}}\sqrt{\frac{2k\left|d_{z0q,2}\right|}{\ln\left(\frac{r_o}{r_i}\right)}}\frac{\left[-\frac{r_i}{\xi_{0q,2}}L_0\left(\xi_{0q,2}\frac{\rho}{r_i}\right)\right]_{r_i}^{r_{o,1}}}{\sqrt{\left[r_i^2L_1\left(\xi_{0q,2}\right)L_1\left(\xi_{0q,2}\right)-r_o^2L_1\left(\xi_{0q,2}\frac{r_o}{r_i}\right)L_1\left(\xi_{0q,2}\frac{r_o}{r_i}\right)\right]}}
\end{aligned}
\tag{2.14}
$$

Here we have made use of the following integral relation for the function $L_k\left(\alpha x\right)$:

$$
\int L_1\left(\alpha x\right)dx = -\frac{L_0\left(\alpha x\right)}{\alpha} \tag{2.15}
$$

The quantities $\{r_{o,1}, r_{o,2}\}$ represent the outer circular coaxial radius for the first- and second-coming waveguide cross-section, whilst $\{r_i\}$ represents the common inner circular coaxial radius between the two waveguide geometries. In addition, the superscript $\{*\}$ represents the complex conjugation operator.

For case (2) $\{\boldsymbol{A_2}\subset\boldsymbol{A_1}\}$ of the aforementioned tangential boundary conditions, where we propagate from a coaxial circular waveguide with a larger to a smaller outer radius, we obtain the following result for the mode-coupling matrix $\mathbf{C}$:

$$
\begin{aligned}
C_{ij} &= \frac{1}{2}\int_{A_2}\left(\boldsymbol{E}_{ti}^{(1)}\times\boldsymbol{H}_{tj}^{(2)*}\right)\cdot\hat{\mathbf{z}}ds \\
&= \frac{1}{2}\int_{A_2}\left(\boldsymbol{E}_{t0n}^{(1)}\times\boldsymbol{H}_{t00}^{(2)*}\right)\cdot\hat{\mathbf{z}}ds \\
&= \frac{1}{2}\int_{A_2}\left(\boldsymbol{E}_{t0n}^{\mathrm{D}(1)}(\boldsymbol{\rho})\times\boldsymbol{H}_{t00}^{\mathrm{D}(2)*}(\boldsymbol{\rho})\right)\cdot\hat{\mathbf{z}}ds \\
&= \frac{1}{2}\int_{A_2}\left(\boldsymbol{e}_{0n}^{\mathrm{D}(1)}(\boldsymbol{\rho})\times\frac{1}{\eta D_0}\boldsymbol{h}_{00}^{\mathrm{D}(2)}(\boldsymbol{\rho})\right)\cdot\hat{\mathbf{z}}ds \\
&= \mp\frac{\xi_{0n,1}}{2\pi r_i d_{t0n,1}}\sqrt{\frac{2\left|d_{z0n,1}\right|}{k\ln\left(\frac{r_o}{r_i}\right)}}\frac{\displaystyle\int_0^{2\pi}\int_{r_i}^{r_{o,2}}L_1\left(\xi_{0n,1}\frac{\rho}{r_i}\right)d\rho d\varphi}{\sqrt{\left[r_i^2L_1\left(\xi_{0n,1}\right)L_1\left(\xi_{0n,1}\right)-r_o^2L_1\left(\xi_{0n,1}\frac{r_o}{r_i}\right)L_1\left(\xi_{0n,1}\frac{r_o}{r_i}\right)\right]}} \\
&= \mp\frac{\xi_{0n,1}}{2\pi r_i d_{t0n,1}}\sqrt{\frac{2\left|d_{z0n,1}\right|}{k\ln\left(\frac{r_o}{r_i}\right)}}\frac{\left[-\frac{r_i}{\xi_{0n,1}}L_0\left(\xi_{0n,1}\frac{\rho}{r_i}\right)\right]_{r_i}^{r_{o,2}}}{\sqrt{\left[r_i^2L_1\left(\xi_{0n,1}\right)L_1\left(\xi_{0n,1}\right)-r_o^2L_1\left(\xi_{0n,1}\frac{r_o}{r_i}\right)L_1\left(\xi_{0n,1}\frac{r_o}{r_i}\right)\right]}}
\end{aligned}
\tag{2.16}
$$

Here we have made use of the same properties as for the aforementioned case. Note that the only difference with the mode-coupling matrix $\mathbf{C}$ between the two cases (1) $\{\boldsymbol{A_1} \subset \boldsymbol{A_2}\}$ and (2) $\{\boldsymbol{A_2} \subset \boldsymbol{A_1}\}$ is the integration cross-section and limits, along with argument in the function $J_k(\alpha x)$ and the function and medium constants.

2.3 TM-TM modal field coupling at a junction between a circular coaxial waveguide and a circular waveguide (without an inner conductor) of the same outer radii.

In subsection 2.3, we make use of equations and properties derived in Appendix B. For case (1) $\{\boldsymbol{A_1} \subset \boldsymbol{A_2}\}$ of the aforementioned tangential boundary conditions, where we propagate from a circular coaxial waveguide to a circular waveguide, we obtain the following result for the mode-coupling matrix $\mathbf{C}$:

$$
\begin{aligned}
C_{ij} &= \frac{1}{2}\int_{A_1}\left(\boldsymbol{E}_{ti}^{(1)}\times\boldsymbol{H}_{tj}^{(2)*}\right)\cdot\hat{\mathbf{z}}ds \\
&= \frac{1}{2}\int_{A_1}\left(\boldsymbol{E}_{t0n}^{(1)}\times\boldsymbol{H}_{t0q}^{(2)*}\right)\cdot\hat{\mathbf{z}}ds \\
&= \frac{1}{2}\int_{A_1}\left(\boldsymbol{E}_{t0n}^{\mathrm{D}(1)}(\boldsymbol{\rho})\times\boldsymbol{H}_{t0q}^{\mathrm{D}(2)*}(\boldsymbol{\rho})\right)\cdot\hat{\mathbf{z}}ds \\
&= \frac{1}{2}\int_{A_1}\left(\boldsymbol{e}_{0n}^{\mathrm{D}(1)}(\boldsymbol{\rho})\times\frac{k}{\eta d_{z0q,2}^{*}}\boldsymbol{h}_{0q}^{\mathrm{D}(2)}(\boldsymbol{\rho})\right)\cdot\hat{\mathbf{z}}ds \\
&= \frac{\xi_{0n,1}\xi_{0q,2}}{\pi r_i r_o^2 d_{t0n,1}d_{t0q,2}d_{z0q,2}^{*}}\sqrt{\frac{|d_{z0n,1}|\,|d_{z0q,2}|}{\left[r_i^2L_{-1}(\xi_{0n,1})L_1(\xi_{0n,1})-r_o^2L_{-1}\left(\xi_{0n,1}\frac{r_o}{r_i}\right)L_1\left(\xi_{0n,1}\frac{r_o}{r_i}\right)\right]J_1^2(\xi_{0q,2})}} \\
&\quad\times\int_0^{2\pi}\int_{r_i}^{r_o}\rho L_1\left(\xi_{0n,1}\frac{\rho}{r_i}\right)J_1\left(\xi_{0q,2}\frac{\rho}{r_o}\right)d\rho d\varphi \\
&= \frac{2\xi_{0n,1}\xi_{0q,2}}{r_i r_o^2 d_{t0n,1}d_{t0q,2}d_{z0q,2}^{*}}\sqrt{\frac{|d_{z0n,1}|\,|d_{z0q,2}|}{\left[r_o^2L_1\left(\xi_{0n,1}\frac{r_o}{r_i}\right)L_1\left(\xi_{0n,1}\frac{r_o}{r_i}\right)-r_i^2L_1(\xi_{0n,1})L_1(\xi_{0n,1})\right]J_1^2(\xi_{0q,2})}} \\
&\quad\times\left[\frac{\xi_{0n,1}\frac{\rho}{r_i}L_2\left(\xi_{0n,1}\frac{\rho}{r_i}\right)J_1\left(\xi_{0q,2}\frac{\rho}{r_o}\right)-\xi_{0q,2}\frac{\rho}{r_o}L_1\left(\xi_{0n,1}\frac{\rho}{r_i}\right)J_2\left(\xi_{0q,2}\frac{\rho}{r_o}\right)}{\frac{\xi_{0n,1}^2}{r_i^2}-\frac{\xi_{0q,2}^2}{r_o^2}}\right]_{r_i}^{r_o}
\end{aligned}
\tag{2.17}
$$

Here we have made use of the relationship $\left\{|x|=\sqrt{xx^*}\right\}$ for complex/imaginary-valued components, the relationship $\left\{L_{-k}(x)=(-1)^k L_k(x)\right\}$, along with the following integral relation for the superposition of the first and second kind Bessel functions:

$$
\int xL_k(\alpha x)J_k(\beta x)\,dx = \frac{\alpha xL_{k+1}(\alpha x)J_k(\beta x)-\beta xL_k(\alpha x)J_{k+1}(\beta x)}{\alpha^2-\beta^2} \tag{2.18}
$$

The quantity $\{r_o\}$ represents the common outer radius for the circular and circular coaxial waveguide cross-section, whilst $\{r_i\}$ represents the inner circular coaxial waveguide radius. Remember that a circular waveguide does not have an inner radius. In addition, the superscript $\{*\}$ represents the complex conjugation operator.

For case (2) $\{\boldsymbol{A_2} \subset \boldsymbol{A_1}\}$ of the aforementioned tangential boundary conditions, where we propagate from a circular waveguide to a circular coaxial waveguide, we obtain the following result for the mode-

coupling matrix $\mathbf{C}$:

$$
\begin{aligned}
C_{ij} &= \frac{1}{2}\int_{A_2}\left(\boldsymbol{E}_{ti}^{(1)}\times\boldsymbol{H}_{tj}^{(2)*}\right)\cdot\hat{\mathbf{z}}ds \\
&= \frac{1}{2}\int_{A_2}\left(\boldsymbol{E}_{t0n}^{(1)}\times\boldsymbol{H}_{t0q}^{(2)*}\right)\cdot\hat{\mathbf{z}}ds \\
&= \frac{1}{2}\int_{A_2}\left(\boldsymbol{E}_{t0n}^{\mathrm{D}(1)}(\boldsymbol{\rho})\times\boldsymbol{H}_{t0q}^{\mathrm{D}(2)*}(\boldsymbol{\rho})\right)\cdot\hat{\mathbf{z}}ds \\
&= \frac{1}{2}\int_{A_2}\left(\boldsymbol{e}_{0n}^{\mathrm{D}(1)}(\boldsymbol{\rho})\times\frac{k}{\eta d_{z0q,2}^{*}}\boldsymbol{h}_{0q}^{\mathrm{D}(2)}(\boldsymbol{\rho})\right)\cdot\hat{\mathbf{z}}ds \\
&= \frac{\xi_{0n,1}\xi_{0q,2}}{\pi r_i r_o^2 d_{t0n,1}d_{t0q,2}d_{z0q,2}^{*}}\sqrt{\frac{|d_{z0n,1}|\,|d_{z0q,2}|}{\left[r_i^2L_{-1}\left(\xi_{0q,2}\right)L_1\left(\xi_{0q,2}\right)-r_o^2L_{-1}\left(\xi_{0q,2}\frac{r_o}{r_i}\right)L_1\left(\xi_{0q,2}\frac{r_o}{r_i}\right)\right]J_1^2\left(\xi_{0n,1}\right)}} \\
&\quad\times\int_0^{2\pi}\int_0^{r_o}\rho L_1\left(\xi_{0q,2}\frac{\rho}{r_i}\right)J_1\left(\xi_{0n,1}\frac{\rho}{r_o}\right)d\rho d\varphi \\
&= \frac{2\xi_{0n,1}\xi_{0q,2}}{r_i r_o^2 d_{t0n,1}d_{t0q,2}d_{z0q,2}^{*}}\sqrt{\frac{|d_{z0n,1}|\,|d_{z0q,2}|}{\left[r_o^2L_1\left(\xi_{0q,2}\frac{r_o}{r_i}\right)L_1\left(\xi_{0q,2}\frac{r_o}{r_i}\right)-r_i^2L_1\left(\xi_{0q,2}\right)L_1\left(\xi_{0q,2}\right)\right]J_1^2\left(\xi_{0n,1}\right)}} \\
&\quad\times\left[\frac{\xi_{0q,2}\frac{\rho}{r_i}L_2\left(\xi_{0q,2}\frac{\rho}{r_i}\right)J_1\left(\xi_{0n,1}\frac{\rho}{r_o}\right)-\xi_{0n,1}\frac{\rho}{r_o}L_1\left(\xi_{0q,2}\frac{\rho}{r_i}\right)J_2\left(\xi_{0n,1}\frac{\rho}{r_o}\right)}{\frac{\xi_{0q,2}^2}{r_i^2}-\frac{\xi_{0n,1}^2}{r_o^2}}\right]_0^{r_o}
\end{aligned}
\tag{2.19}
$$

Here we have made use of the same properties as for the aforementioned case. Note that the only difference with the mode-coupling matrix $\mathbf{C}$ between the two cases (1) $\{\boldsymbol{A_1}\subset\boldsymbol{A_2}\}$ and (2) $\{\boldsymbol{A_2}\subset\boldsymbol{A_1}\}$ is the arguments between the functions $L_k\left(\alpha x\right)$ and $J_k\left(\beta x\right)$.

2.4 TEM-TM modal field coupling at a junction between a circular coaxial waveguide and a circular waveguide (without an inner conductor) of the same outer radii.

In subsection 2.4, we make use of equations and properties derived in Appendix A and B. For case (1) $\{\boldsymbol{A_1}\subset\boldsymbol{A_2}\}$ of the aforementioned tangential boundary conditions, where we propagate from a circular coaxial waveguide to a circular waveguide, we obtain the following result for the mode-coupling matrix $\mathbf{C}$:

$$
\begin{aligned}
C_{ij} &= \frac{1}{2}\int_{A_1}\left(\boldsymbol{E}_{ti}^{(1)}\times\boldsymbol{H}_{tj}^{(2)*}\right)\cdot\hat{\mathbf{z}}ds \\
&= \frac{1}{2}\int_{A_1}\left(\boldsymbol{E}_{t00}^{(1)}\times\boldsymbol{H}_{t0q}^{(2)*}\right)\cdot\hat{\mathbf{z}}ds \\
&= \frac{1}{2}\int_{A_1}\left(\boldsymbol{E}_{t00}^{\mathrm{D}(1)}(\boldsymbol{\rho})\times\boldsymbol{H}_{t0q}^{\mathrm{D}(2)*}(\boldsymbol{\rho})\right)\cdot\hat{\mathbf{z}}ds \\
&= \frac{1}{2}\int_{A_1}\left(\frac{1}{D_0}\boldsymbol{e}_{00}^{\mathrm{D}(1)}(\boldsymbol{\rho})\times\frac{k}{\eta d_{z0q,2}^{*}}\boldsymbol{h}_{0q}^{\mathrm{D}(2)}(\boldsymbol{\rho})\right)\cdot\hat{\mathbf{z}}ds \\
&= \mp\frac{\xi_{0q,2}}{2\pi r_o^2 d_{t0q,2}d_{z0q,2}^{*}J_1\left(\xi_{0q,2}\right)}\sqrt{\frac{2k\,|d_{z0q,2}|}{\ln\left(\frac{r_o}{r_i}\right)}}\int_0^{2\pi}\int_{r_i}^{r_o}J_1\left(\xi_{0q,2}\frac{\rho}{r_o}\right)d\rho d\varphi \\
&= \mp\frac{\xi_{0q,2}}{r_o^2 d_{t0q,2}d_{z0q,2}^{*}J_1\left(\xi_{0q,2}\right)}\sqrt{\frac{2k\,|d_{z0q,2}|}{\ln\left(\frac{r_o}{r_i}\right)}}\left[-\frac{r_o}{\xi_{0q,2}}J_1\left(\xi_{0q,2}\frac{\rho}{r_o}\right)\right]_{r_i}^{r_o}
\end{aligned}
\tag{2.20}
$$

Here we have made use of the following integral relation between the first and zeroth order Bessel function of the first kind $J_k(\alpha x)$:

$$\int J_1(\alpha x)\,dx = -\frac{J_0(\alpha x)}{\alpha} \tag{2.21}$$

The quantity $\{r_o\}$ represents the common outer radius for the circular and circular coaxial waveguide cross-section, whilst $\{r_i\}$ represents the inner circular coaxial waveguide radius. Remember that a circular waveguide does not have an inner radius. In addition, the superscript $\{*\}$ represents the complex conjugation operator.

For case (2) $\{\boldsymbol{A_2} \subset \boldsymbol{A_1}\}$ of the aforementioned tangential boundary conditions, where we propagate from a circular waveguide to a circular coaxial waveguide, we obtain the following result for the mode-coupling matrix $\mathbf{C}$:

$$\begin{aligned}
C_{ij} &= \frac{1}{2}\int_{A_2}\left(\boldsymbol{E}_{ti}^{(1)} \times \boldsymbol{H}_{tj}^{(2)*}\right)\cdot\hat{\mathbf{z}}ds \\
&= \frac{1}{2}\int_{A_2}\left(\boldsymbol{E}_{t0n}^{(1)} \times \boldsymbol{H}_{t00}^{(2)*}\right)\cdot\hat{\mathbf{z}}ds \\
&= \frac{1}{2}\int_{A_2}\left(\boldsymbol{E}_{t0n}^{\mathrm{D}(1)}(\boldsymbol{\rho}) \times \boldsymbol{H}_{t00}^{\mathrm{D}(2)*}(\boldsymbol{\rho})\right)\cdot\hat{\mathbf{z}}ds \\
&= \frac{1}{2}\int_{A_2}\left(\boldsymbol{e}_{0n}^{\mathrm{D}(1)}(\boldsymbol{\rho}) \times \frac{1}{\eta D_0}\boldsymbol{h}_{00}^{\mathrm{D}(2)}(\boldsymbol{\rho})\right)\cdot\hat{\mathbf{z}}ds \\
&= \mp\frac{\xi_{0n,1}}{2\pi r_o^2 d_{t0n,1} J_1(\xi_{0n,1})}\sqrt{\frac{2\left|d_{z0n,1}\right|}{k\ln\left(\frac{r_o}{r_i}\right)}}\int_0^{2\pi}\int_0^{r_o} J_1\left(\xi_{0n,1}\frac{\rho}{r_o}\right)d\rho d\varphi \\
&= \mp\frac{\xi_{0n,1}}{r_o^2 d_{t0n,1} J_1(\xi_{0n,1})}\sqrt{\frac{2\left|d_{z0n,1}\right|}{k\ln\left(\frac{r_o}{r_i}\right)}}\left[-\frac{r_o}{\xi_{0n,1}}J_0\left(\xi_{0n,1}\frac{\rho}{r_o}\right)\right]_0^{r_o}
\end{aligned} \tag{2.22}$$

Here we have made use of the same properties as for the aforementioned case. Note that the only difference with the mode-coupling matrix $\mathbf{C}$ between the two cases (1) $\{\boldsymbol{A_1} \subset \boldsymbol{A_2}\}$ and (2) $\{\boldsymbol{A_2} \subset \boldsymbol{A_1}\}$ is the integration cross-section and limits, along with argument in the Bessel function of the first kind $J_k(\alpha x)$ and the function and medium constants.

Using the tensor formulation of the aforementioned quantities, we could construct a linear equation system in order to obtain the scattering matrix $\mathbf{S}$ at a cross-sectional waveguide junction as follows:

$$\left.\begin{aligned}
\mathbf{D}_2\left[\boldsymbol{a}^+(z_2) + \boldsymbol{a}^-(z_2)\right] &= \mathbf{C}^{\mathrm{T}}\left[\boldsymbol{a}^+(z_1) + \boldsymbol{a}^-(z_1)\right] \\
\mathbf{D}_1^*\left[\boldsymbol{a}^+(z_1) - \boldsymbol{a}^-(z_1)\right] &= \mathbf{C}^*\left[\boldsymbol{a}^+(z_2) - \boldsymbol{a}^-(z_2)\right]
\end{aligned}\right\} \tag{2.23}$$

$$\begin{bmatrix}\boldsymbol{a}^-(z_1)\\ \boldsymbol{a}^+(z_2)\end{bmatrix} = \begin{bmatrix}\mathbf{S}_{11} & \mathbf{S}_{12}\\ \mathbf{S}_{21} & \mathbf{S}_{22}\end{bmatrix}\begin{bmatrix}\boldsymbol{a}^+(z_1)\\ \boldsymbol{a}^-(z_2)\end{bmatrix} \tag{2.24}$$

Here the superscript T and $*$ represent the transpose and the conjugate of a tensor respectively. The general expression for the scattering coefficients $\mathbf{S}_{uv}$, where $\{u, v = 1, 2\}$, at a cross-sectional waveguide junction could be expressed as follows

$$\mathbf{S}_{11} = \left(\mathbf{D}_1^* + \mathbf{C}^*\mathbf{D}_2^{-1}\mathbf{C}^{\mathrm{T}}\right)^{-1}\left(\mathbf{D}_1^* - \mathbf{C}^*\mathbf{D}_2^{-1}\mathbf{C}^{\mathrm{T}}\right) \tag{2.25}$$

$$\mathbf{S}_{12} = 2\left(\mathbf{D}_1^* + \mathbf{C}^*\mathbf{D}_2^{-1}\mathbf{C}^{\mathrm{T}}\right)^{-1}\mathbf{C}^* \tag{2.26}$$

$$\mathbf{S}_{21} = 2\left(\mathbf{C}^{\mathrm{T}}\left(\mathbf{D}_1^*\right)^{-1}\mathbf{C}^* + \mathbf{D}_2\right)^{-1}\mathbf{C}^{\mathrm{T}} \tag{2.27}$$

$$\mathbf{S}_{22} = \left(\mathbf{C}^{\mathrm{T}} \left(\mathbf{D}_1^*\right)^{-1} \mathbf{C}^* + \mathbf{D}_2\right)^{-1} \left(\mathbf{C}^{\mathrm{T}} \left(\mathbf{D}_1^*\right)^{-1} \mathbf{C}^* - \mathbf{D}_2\right) \tag{2.28}$$

The cascading of scattering matrices is exemplified using Figure 2 below. The two scattering systems, denoted L and R, could each represent a cross-sectional waveguide junction along with a uniform propagation section.

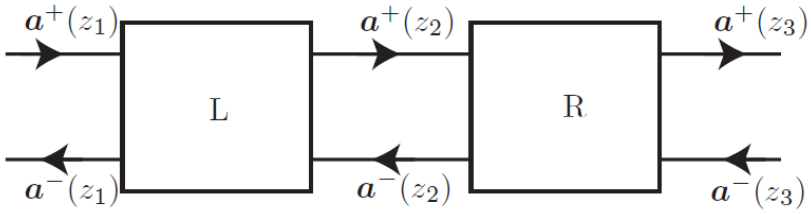

Figure 2: Cascading of two scattering systems.

Their scattering matrices for the two systems are denoted $\mathbf{S}_{\mathrm{L}}$ and $\mathbf{S}_{\mathrm{R}}$ and could be represented in their tensor notation as follows:

$$\begin{bmatrix} \boldsymbol{a}^-(z_1) \\ \boldsymbol{a}^+(z_2) \end{bmatrix} = \begin{bmatrix} \mathbf{S}_{11}^{\mathrm{L}} & \mathbf{S}_{12}^{\mathrm{L}} \\ \mathbf{S}_{21}^{\mathrm{L}} & \mathbf{S}_{22}^{\mathrm{L}} \end{bmatrix} \begin{bmatrix} \boldsymbol{a}^+(z_1) \\ \boldsymbol{a}^-(z_2) \end{bmatrix} \tag{2.29}$$

$$\begin{bmatrix} \boldsymbol{a}^-(z_2) \\ \boldsymbol{a}^+(z_3) \end{bmatrix} = \begin{bmatrix} \mathbf{S}_{22}^{\mathrm{R}} & \mathbf{S}_{23}^{\mathrm{R}} \\ \mathbf{S}_{32}^{\mathrm{R}} & \mathbf{S}_{33}^{\mathrm{R}} \end{bmatrix} \begin{bmatrix} \boldsymbol{a}^+(z_2) \\ \boldsymbol{a}^-(z_3) \end{bmatrix} \tag{2.30}$$

The cascaded scattering matrix for the entire waveguiding system could be expressed in tensor notation as follows:

$$\begin{bmatrix} \boldsymbol{a}^-(z_1) \\ \boldsymbol{a}^+(z_3) \end{bmatrix} = \begin{bmatrix} \mathbf{S}_{11} & \mathbf{S}_{13} \\ \mathbf{S}_{31} & \mathbf{S}_{33} \end{bmatrix} \begin{bmatrix} \boldsymbol{a}^+(z_1) \\ \boldsymbol{a}^-(z_3) \end{bmatrix} \tag{2.31}$$

Here, the scattering coefficients of the cascaded scattering matrix could be expressed as follows:

$$\mathbf{S}_{11} = \mathbf{S}_{11}^{\mathrm{L}} + \mathbf{S}_{12}^{\mathrm{L}} \left(\mathbf{I} - \mathbf{S}_{22}^{\mathrm{R}} \mathbf{S}_{22}^{\mathrm{L}}\right)^{-1} \mathbf{S}_{22}^{\mathrm{R}} \mathbf{S}_{21}^{\mathrm{L}} \tag{2.32}$$

$$\mathbf{S}_{13} = \mathbf{S}_{12}^{\mathrm{L}} \left(\mathbf{I} - \mathbf{S}_{22}^{\mathrm{R}} \mathbf{S}_{22}^{\mathrm{L}}\right)^{-1} \mathbf{S}_{23}^{\mathrm{R}} \tag{2.33}$$

$$\mathbf{S}_{31} = \mathbf{S}_{32}^{\mathrm{R}} \left(\mathbf{I} - \mathbf{S}_{22}^{\mathrm{L}} \mathbf{S}_{22}^{\mathrm{R}}\right)^{-1} \mathbf{S}_{21}^{\mathrm{L}} \tag{2.34}$$

$$\mathbf{S}_{33} = \mathbf{S}_{33}^{\mathrm{R}} + \mathbf{S}_{32}^{\mathrm{R}} \left(\mathbf{I} - \mathbf{S}_{22}^{\mathrm{L}} \mathbf{S}_{22}^{\mathrm{R}}\right)^{-1} \mathbf{S}_{22}^{\mathrm{L}} \mathbf{S}_{23}^{\mathrm{R}} \tag{2.35}$$

The propagator matrix $\mathbf{P}$ describes the longitudinal wave propagation between cross-sectional waveguide junctions, where the waveguiding system is assumed uniform and source-free. The propagation coefficients are related to the expansion coefficients $\{\boldsymbol{a}^+(z), \boldsymbol{a}^-(z)\}$ as follows:

$$a_{0n}^+(z_\beta) = a_{0n}^+(z_\alpha) e^{-jd_{z0n}(z_\beta - z_\alpha)} \tag{2.36}$$

$$a_{0n}^-(z_\alpha) = a_{0n}^+(z_\beta) e^{jd_{z0n}(z_\alpha - z_\beta)} \tag{2.37}$$

In reference to Figure 2 above, we have that $\{z_\alpha, z_\beta\}$ are two points between the cross-sectional waveguide junctions L and R in the scattering system, and $d_{zi} = d_{z0n}$ depend on the waveguide geometry between the points $\{z_\alpha, z_\beta\}$. The propagation coefficients could now be expressed as follows:

$$\begin{aligned} P_{ij} &= \delta_{ij} e^{-jd_{zi}(z_\alpha - z_\beta)} \\ &= \delta_{0n}\delta_{0q} e^{-jd_{z0n}(z_\alpha - z_\beta)} \end{aligned} \tag{2.38}$$

The propagator matrix $\mathbf{P}$ between cross-sectional waveguide junctions L and R could be expressed in tensor notation as follows:

$$\begin{bmatrix} \boldsymbol{a}^-(z_1) \\ \boldsymbol{a}^+(z_2) \end{bmatrix} = \begin{bmatrix} \mathbf{0} & \mathbf{P} \\ \mathbf{P} & \mathbf{0} \end{bmatrix} \begin{bmatrix} \boldsymbol{a}^+(z_1) \\ \boldsymbol{a}^-(z_2) \end{bmatrix} \tag{2.39}$$

A more explicit representation of the scattering matrices $\mathbf{S}_{\mathrm{L}}$ and $\mathbf{S}_{\mathrm{R}}$ for the aforementioned systems denoted L and R, each representing a cross-sectional waveguide junction along with a uniform propagation section, could be the following:

$$\begin{aligned}\begin{bmatrix}\boldsymbol{a}^{-}(z_1)\\ \boldsymbol{a}^{+}(z_2)\end{bmatrix} &= \begin{bmatrix}\mathbf{S}_{11}^{\mathrm{L}} & \mathbf{S}_{12}^{\mathrm{L}}\\ \mathbf{S}_{21}^{\mathrm{L}} & \mathbf{S}_{22}^{\mathrm{L}}\end{bmatrix}\begin{bmatrix}\boldsymbol{a}^{+}(z_1)\\ \boldsymbol{a}^{-}(z_2)\end{bmatrix}\\ &= \begin{bmatrix}\mathbf{S}_{11} & \mathbf{S}_{12}\\ \mathbf{S}_{21} & \mathbf{S}_{22}\end{bmatrix}\begin{bmatrix}\mathbf{0} & \mathbf{P}_{\mathrm{L}}\\ \mathbf{P}_{\mathrm{L}} & \mathbf{0}\end{bmatrix}\begin{bmatrix}\boldsymbol{a}^{+}(z_1)\\ \boldsymbol{a}^{-}(z_2)\end{bmatrix}\end{aligned} \tag{2.40}$$

$$\begin{aligned}\begin{bmatrix}\boldsymbol{a}^{-}(z_2)\\ \boldsymbol{a}^{+}(z_3)\end{bmatrix} &= \begin{bmatrix}\mathbf{S}_{22}^{\mathrm{R}} & \mathbf{S}_{23}^{\mathrm{R}}\\ \mathbf{S}_{32}^{\mathrm{R}} & \mathbf{S}_{33}^{\mathrm{R}}\end{bmatrix}\begin{bmatrix}\boldsymbol{a}^{+}(z_2)\\ \boldsymbol{a}^{-}(z_3)\end{bmatrix}\\ &= \begin{bmatrix}\mathbf{S}_{22} & \mathbf{S}_{23}\\ \mathbf{S}_{32} & \mathbf{S}_{33}\end{bmatrix}\begin{bmatrix}\mathbf{0} & \mathbf{P}_{\mathrm{R}}\\ \mathbf{P}_{\mathrm{R}} & \mathbf{0}\end{bmatrix}\begin{bmatrix}\boldsymbol{a}^{+}(z_2)\\ \boldsymbol{a}^{-}(z_3)\end{bmatrix}\end{aligned} \tag{2.41}$$

Here we have that $\mathbf{P}_{\mathrm{L}}$ and $\mathbf{P}_{\mathrm{R}}$ represents propagator matrices for the wave propagation within a uniform propagating section for each of the aforementioned scattering systems. In our case, the propagator matrix $\mathbf{P}$ will represent the wave propagation between cross-sectional waveguiding junctions in the loaded cavity. By following the propagation direction in the loaded cavity, the complete scattering matrix $\mathbf{S}_{\mathrm{loaded}}$ could be determined iteratively. Primarily, we determine the scattering matrix at the first cross-sectional waveguide junction. Secondarily, we multiply the calculated scattering matrix by the propagator matrix, which is incorporated to account for the wave propagation between the current and the forthcoming cross-sectional waveguide junction. Tertiarily, we cascade the scattering system from the second step with the forthcoming cross-sectional waveguide junction and obtain a new scattering matrix. We repeat the second and third steps until we have iterated through the entire loaded cavity structure, which results in calculating the complete loaded scattering matrix $\mathbf{S}_{\mathrm{loaded}}$.

3 Determine the loaded Q-values at the resonance frequencies.

The loaded Q-values at the TM_{0n}-mode resonance frequencies for the loaded cavity system are determined using the scattering matrix $\mathbf{S}$ and the scattering coefficients $\mathbf{S}_{uv}$, where $\{u, v = 1, 4\}$, which have been introduced and documented in Section 2. The loaded Q-values are determined by obtaining the TM-mode resonance frequencies from the transmission scattering coefficient $\mathbf{S}_{14}$ and then dividing these TM-mode resonance frequencies by their respective 3-dB bandwidths. The Q-values at the TM_{0n}-mode resonance frequencies for the loaded cavity system could be expressed as follows:

$$\begin{aligned} Q_{loaded} &= \frac{\omega_{res}}{BW_{3-dB}} \\ &= \frac{\omega_{res}}{\omega^{+}_{3-dB} - \omega^{-}_{3-dB}} \end{aligned} \tag{3.1}$$

Here we have that ω_{res} represents the TM_{0n}-mode resonance frequencies, whilst $\{\omega^{+}_{3-dB}, \omega^{-}_{3-dB}\}$ represent the upper and lower frequencies of the 3-dB bandwidth for the given TM_{0n}-mode resonance frequencies respectively.

4 Determine the current distributions on the probes and compare them with the standing wave approximation.

The current distribution on the probes is determined using the power normalized magnetic field expressions from Appendix B and C, along with the description of the scattering matrix $\mathbf{S}$ and the scattering coefficients $\mathbf{S}_{uv}$, where $\{u, v = 1, 5\}$, which have been introduced and documented in Section 2. The complete scattering matrix $\mathbf{S}_{\text{loaded}}$ for the loaded cavity could be expressed as follows:

$$\begin{bmatrix} \boldsymbol{a}^-(z_1) \\ \boldsymbol{a}^+(z_5) \end{bmatrix} = \begin{bmatrix} \mathbf{S}_{11} & \mathbf{S}_{15} \\ \mathbf{S}_{51} & \mathbf{S}_{55} \end{bmatrix} \begin{bmatrix} \boldsymbol{a}^+(z_1) \\ \boldsymbol{a}^-(z_5) \end{bmatrix} \tag{4.1}$$

Here we have that the indices 1 and 5 represent the first and last waveguiding sections in the loaded cavity structure. We proceed by assuming the following: (1) no power is reflected back to the source in the first waveguiding section $\{\boldsymbol{a}^-(z_1) = \mathbf{0}\}$; (2) all incident power is transmitted in the first waveguiding section $\{\boldsymbol{a}^+(z_1) = \mathbf{1}\}$; and (3) the loaded cavity is impedance-matched or infinitely long in the last waveguiding section $\{\boldsymbol{a}^-(z_5) = \mathbf{0}\}$. The loaded scattering matrix $\mathbf{S}_{\text{loaded}}$ could now be expressed as follows:

$$\begin{bmatrix} \mathbf{0} \\ \boldsymbol{a}^+(z_5) \end{bmatrix} = \begin{bmatrix} \mathbf{S}_{11} & \mathbf{S}_{15} \\ \mathbf{S}_{51} & \mathbf{S}_{55} \end{bmatrix} \begin{bmatrix} \mathbf{1} \\ \mathbf{0} \end{bmatrix} \tag{4.2}$$

The loaded scattering matrix $\mathbf{S}_{\text{loaded}}$ now results with the following expression:

$$\begin{aligned} \boldsymbol{a}^+(z_5) &= \mathbf{S}_{51} \\ &= \sum_{i=1}^{\infty} \mathrm{S}_{51i}\left(\omega, z\right) \end{aligned} \tag{4.3}$$

By considering the aforementioned assumptions, the total power normalized magnetic field in the loaded cavity could be expressed as follows:

$$\boldsymbol{H}_{\text{tot}}(\mathbf{r}) = \sum_{i=1}^{\infty} \mathrm{S}_{51i}\left(\omega, z\right) \left[\boldsymbol{H}_i^{\text{D, Coax}}(\boldsymbol{\rho}) + \boldsymbol{H}_i^{\text{D, Circ}}(\boldsymbol{\rho})\right] \tag{4.4}$$

Here we have that denote $i = mn$ as a collective term for variable parameters, which is introduced for convenience. The transversal magnetic TM_{0n}-modal field expressions $\left\{\boldsymbol{H}_{0n}^{\text{D, Coax}}(\boldsymbol{\rho}), \boldsymbol{H}_{0n}^{\text{D, Circ}}(\boldsymbol{\rho})\right\}$, and the transverse electromagnetic TEM modal field expression $\boldsymbol{H}_{00}^{\text{D, Coax}}(\boldsymbol{\rho})$, are defined as follows:

$$\boldsymbol{H}_{0n}^{\text{D, Coax}\pm}(\boldsymbol{\rho}) = \mp\hat{\boldsymbol{\varphi}}\frac{\xi_{0n}^{\text{Coax}}}{r_i d_{t0n}^{\text{Coax}}}\sqrt{\frac{2k}{\pi\eta\left|d_{z0n}^{\text{Coax}}\right|}}\frac{L_1\left(\xi_{0n}^{\text{Coax}}\dfrac{\rho}{r_i}\right)}{\sqrt{\left[r_i^2 L_{-1}\left(\xi_{0n}^{\text{Coax}}\right)L_1\left(\xi_{0n}^{\text{Coax}}\right) - r_o^2 L_{-1}\left(\xi_{0n}^{\text{Coax}}\dfrac{r_o}{r_i}\right)L_1\left(\xi_{0n}^{\text{Coax}}\dfrac{r_o}{r_i}\right)\right]}} \tag{4.5}$$

$$\boldsymbol{H}_{0n}^{\text{D, Circ}\pm}(\boldsymbol{\rho}) = \mp\hat{\boldsymbol{\varphi}}\frac{\xi_{0n}^{\text{Circ}}}{r_o^2 d_{t0n}^{\text{Circ}}}\sqrt{\frac{2k}{\pi\eta\left|d_{z0n}^{\text{Circ}}\right|}}\frac{J_1\left(\xi_{0n}^{\text{Circ}}\dfrac{\rho}{r_o}\right)}{J_1\left(\xi_{0n}^{\text{Circ}}\right)} \tag{4.6}$$

$$\boldsymbol{H}_{00}^{\text{Circ}\pm}(\boldsymbol{\rho}) = \pm\hat{\boldsymbol{\varphi}}\sqrt{\frac{1}{\pi\eta\ln\left(\dfrac{r_o}{r_i}\right)}}\frac{1}{\rho} \tag{4.7}$$

The current distribution on the probes inside the loaded cavity could be described as a surface current

K as follows:

$$
\begin{aligned}
\boldsymbol{K} =& -\hat{\mathbf{n}} \times \boldsymbol{H}_{\mathrm{tot}}^{\mathrm{TM}}(\mathbf{r}) \\
=& -\hat{\boldsymbol{\rho}} \times \sum_{i=0}^{\infty} \mathrm{S}_{51,0n}(\omega, z) \left[\boldsymbol{H}_{0n}^{\mathrm{D,\ Coax}\pm}(\boldsymbol{\rho}) + \boldsymbol{H}_{0n}^{\mathrm{D,\ Circ}\pm}(\boldsymbol{\rho}) \right] \\
=& \pm \hat{\mathbf{z}} \sum_{i=0}^{\infty} \mathrm{S}_{51,0n}(\omega, z) \left[\frac{\xi_{0n}^{\mathrm{Coax}}}{r_i d_{t0n}^{\mathrm{Coax}}} \sqrt{\frac{2k}{\pi\eta \left| d_{z0n}^{\mathrm{Coax}} \right|}} \frac{L_1\left(\xi_{0n}^{\mathrm{Coax}} \dfrac{\rho}{r_i}\right)}{\sqrt{\left[r_i^2 L_{-1}\left(\xi_{0n}^{\mathrm{Coax}}\right) L_1\left(\xi_{0n}^{\mathrm{Coax}}\right) - r_o^2 L_{-1}\left(\xi_{0n}^{\mathrm{Coax}} \dfrac{r_o}{r_i}\right) L_1\left(\xi_{0n}^{\mathrm{Coax}} \dfrac{r_o}{r_i}\right) \right]}} \right. \\
& \left. + \frac{\xi_{0n}^{\mathrm{Circ}}}{r_o^2 d_{t0n}^{\mathrm{Circ}}} \sqrt{\frac{2k}{\pi\eta \left| d_{z0n}^{\mathrm{Circ}} \right|}} \frac{J_1\left(\xi_{0n}^{\mathrm{Circ}} \dfrac{\rho}{r_o}\right)}{J_1\left(\xi_{0n}^{\mathrm{Circ}}\right)} - \sqrt{\frac{1}{\pi\eta \ln\left(\dfrac{r_o}{r_i}\right)}} \frac{1}{\rho} \right]
\end{aligned}
\tag{4.8}
$$

5 Numerical code package

In this section we present a MATLAB code package *CylWaveCascade*[1] that we have written based on the general theory provided by section 2 and Appendices B and C. In short, the package allow calculations of scattering matrices of cylindrical waveguide junctions together with their related propagation matrices. It has been our aim to provide a code that is simple to use, so that each connection of waveguides is essentially a one-line operation. The cascading of X scattering systems is then a simple matter of writing X lines for each junction plus propagator and completing the scattering system with multiplying the matrices together. The code package is thoroughly written from the ground up, including optimized numerical schemes for approximating any number of roots of the various Bessel functions.

5.1 Example: coaxial connector

An example is provided here for the first set of coaxial connectors in Figure 1. The first coaxial has an outer radius b while the second conductor has outer radius R and extends a distance h_2. The coaxials share an inner conductor of radius a. A frequency sweep for N modes can then be calculated as shown in Figure 3. The resulting output matrix S includes the scattering matrix of the junction S_{junc} and the propagator P_2 of the geometry immediately following the junction, i.e. $S = S_{\text{junc}}P_2$. Optionally, the propagator of the first geometry may also be included, in that case, $S = P_1 S_{\text{junc}} P_2$. This option may be useful when comparing results with experimental results or computational simulations where the distance up until the junction may be required to be finite. In short, the function `scattering_matrix_coaxials` calculates the diagonal matrices with (2.10), the coupling matrices with (in this case) equation (2.11), and the propagator matrices with (2.38), taking into account all modes simultaneously. Finally, it checks that the resulting output matrix is physically realizable. The function is computationally efficient with respect to the number of modes to calculate, taking 0.1-0.2 seconds runtime whether it is calculated for a total of 1 or 100 modes.
In Figure 4 we present the reflectance and transmittance found from running the code shown in Figure 3, for three cases where the total number of modes N is one, two, or three. For the TM_{01} mode shown in Figure 4a, we also present the scattering matrix at 5 GHz numerically,

$$\mathbf{S} = \begin{bmatrix} 0.829 - 0.174i & -0.520 + 0.109i \\ 0.520 - 0.109i & 0.829 - 0.174i \end{bmatrix}. \tag{5.1}$$

As higher order modes are included in the calculation in Figures 4b and 4c, the response is severely affected with respect to frequency as coupling between the modes is taken into account. The sudden and discontinuous changes in the response coincide with the onset of the cutoff frequencies of the various modes in each geometry. These cutoff frequencies can be found in Table 1, calculated with (2.1) with $p = 0$. For this simple case we note that the absolute value of the S-parameters squared summed over all modes is equal to 1 in all cases.

```
% A coaxial waveguide consisting of two geometries:
% Coax 1: outer radius b, coax length h_1
% Coax 2: outer radius R, coax length h_2
% Common inner conductor with radius a.

freq = linspace(1, 10, 200).*1e9; % operating frequency
a = 1e-2;
b = 8e-2;
R = 12e-2;
h = 6e-2;
N = 3; % number of modes (highest mode TM_{0N})

S = cell(length(freq),1);
for i=1:length(freq)
    S{i} = scattering_matrix_coaxials(freq(i), a, b, R, 0, h, N);
end
```

Figure 3: Frequency sweep for the three lowest modes of two coaxial connectors.

[1] https://github.com/brageboe/CylWaveCascade

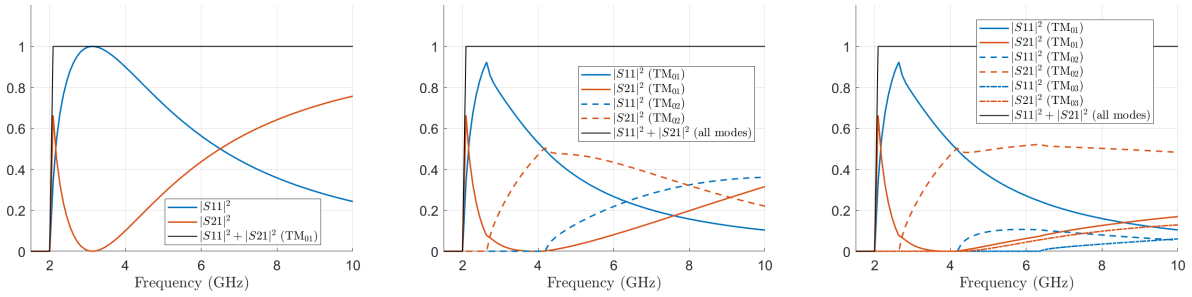

(a) (b) (c)

Figure 4: Reflection and transmission spectra for the two coaxial connectors specified in Fig. 3 when the total number of modes is (a) one (b) two and (c) three.

n	$f_c^{(1)}$	$f_c^{(2)}$
1	2.049	1.285
2	4.220	2.670
3	6.378	4.045

Table 1: Cutoff frequencies in GHz for coaxial 1 with radius $b = 8$ cm and coaxial 2 with radius $R = 12$ cm at given mode TM_{0n}.

5.2 Example: resonator cavity

Another example is of course the resonator cavity described in Figure 1. The short code snippet required to model this cavity using *CylWaveCascade* is depicted in Figure 5. The function `scattering_matrix_coaxials` is again used for the junctions between coaxials, where it automatically detects whether to calculate for case 1 with (2.11), or case 2 with (2.13). The junctions between coaxial and circular waveguides are calculated with `scattering_matrix_mixed`. Here, the user must specify whether we are dealing with case 1 (2.17) or case 2 (2.19). Unless otherwise specified by the user, the output of both functions also includes the propagator matrix of the geometry immediately following the junction.

```
freq = linspace(1, 10, 200).*1e9; % operating frequency
a = 1e-2;
b = 8e-2;
R = 12e-2;
h = 6e-2; % parameter h in Fig.1
d = 18e-2;  % parameter d in Fig.1
N = 3; % number of modes (highest mode TM_{0N})

S1 = cell(length(freq),1);
S2 = S1;
S3 = S1;
S4 = S1;
S = S1;

for i=1:length(freq)
    S1{i} = scattering_matrix_coaxials(freq(i), a, b, R, 0, h, N);
    S2{i} = scattering_matrix_mixed(freq(i), a, R, 0, d-2*h, N, 1);
    S3{i} = scattering_matrix_mixed(freq(i), a, R, 0, h, N, 2);
    S4{i} = scattering_matrix_coaxials(freq(i), a, R, b, 0, h, N, propagator_geometry2=false);
    S{i} = S1{i} * S2{i} * S3{i} * S4{i};
    check_physical_realizability(S{i}, print_warning=false);
end
```

Figure 5: Frequency sweep for the lowest mode for the resonator cavity presented in Fig. 1.

The resonator cavity may be coded as depicted in Figure 5. For the parameter values provided there, reflectance and transmittance spectra found running the code are shown in Figure 6. Clearly, at this point, we are running into problems as the scattering parameters do not sum up to unity at several frequencies. The code base has grown quite large and involves many intricate details that are based on complicated theory, so debugging and troubleshooting can be time-consuming. So the unphysical scattering parameters may certainly be due to numerical problems. At this point, it is important to point out an incompleteness with the current version of *CylWaveCascade*, which is that the theory describing the coupling between TEM and TM modes, sections 2.2 and 2.4, are not yet implemented.

Thus, Figure 6 shows only coupling between TM-TM modes. The reason for the exclusion of TEM-TM coupling is that the development of the theory was completed close to the date of submission, and so due to time constraints, its implementation into *CylWaveCascade* remains as a future update.

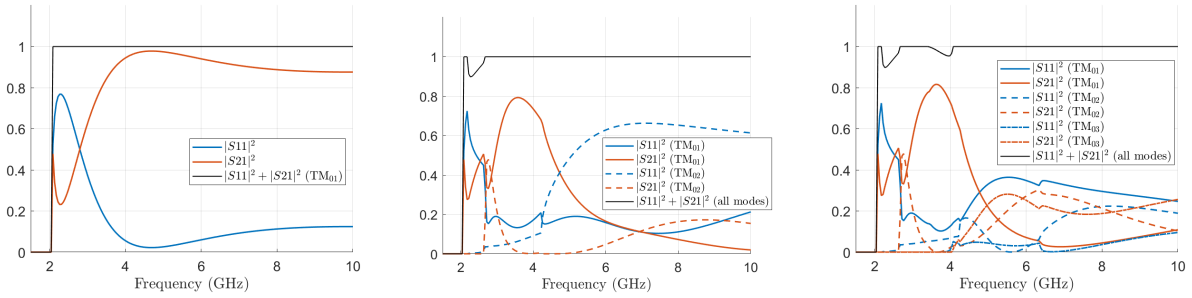

(a) **(b)** **(c)**

Figure 6: Reflection and transmission spectra for the loaded resonator cavity specified in Fig. 5 when the total number of modes is (a) one (b) two and (c) three.

5.3 Outlook

CylWaveCascade currently models the cascading of cylindrical waveguides with and without a central conductor for TM modes. It is a well-documented code package with a solid foundation and functionality that allows relatively easy implementation of further extensions. However, there is still a way to go before a functioning version can be released. Notably is a need for implementing TEM-TM coupling. Otherwise, there are a lot of numerical wrinkles that need ironing out. Crucially is the need for independent verification from simulation software, which could potentially confirm both the theory presented in this report and whether the code is correctly implemented. Several models have been proposed in COMSOL Multiphysics, one of which is depicted in Figure 7. Challenges were also met in COMSOL, where disagreements were found between different solvers (e.g. eigenfrequency solver and frequency domain solvers claiming different resonance frequencies for the same geometries), and the choice of mode excitation was limited. All of the above are areas to focus on for future updates.

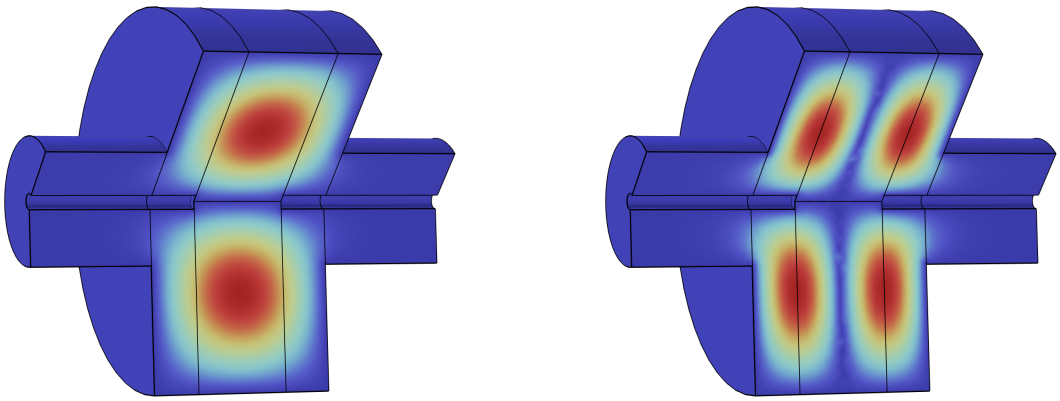

(a) **(b)**

Figure 7: Electric field distribution at two resonance frequencies using an eigenfrequency solver in COMSOL Multiphysics.

Appendix

Appendix A Derive analytical expressions for the dominant TEM-modes in a circular coaxial waveguide.

We proceed to derive the analytical expressions for the electric and magnetic field of TEM-modes in a coaxial waveguide using an eigenvalue problem description. The Dirichlet boundary problem, using the eigenfunction $\phi_0(\boldsymbol{\rho}) = \phi_0(\rho, \varphi)$, for TEM modes in a coaxial waveguide is expressed as follows:

$$\left.\begin{aligned} &\nabla_t^2 \phi_0(\rho, \varphi) = 0 \\ &\phi_0(\rho = r_i, \varphi) = V_0 \\ &\phi_0(\rho = r_o, \varphi) = 0 \end{aligned}\right\} \tag{A.1}$$

Here we have that V_0 is an arbitrary potential on the inner conductor, whilst the outer conductor is grounded. The inner and outer coaxial radii are denoted $\{r_o, r_i\}$ respectively. We start by expressing the Laplace equation explicitly in cylindrical coordinates:

$$\left(\frac{1}{\rho}\frac{\partial}{\partial\rho}\left(\rho\frac{\partial}{\partial\rho}\right) + \frac{1}{\rho^2}\frac{\partial^2}{\partial\varphi^2}\right)\phi_0(\rho, \varphi) = 0 \tag{A.2}$$

We could solve the Laplace equation by using the method of separation of variables. After an appropriate separation ansatz has been chosen and introduced it into Eq.A.2, the resulting expression is then divided by the separation ansatz and multiplied by ρ^2. This is done so that we achieve independent terms for each variable in Eq.A.2.

$$\phi_0(\rho, \varphi) = R(\rho)F(\varphi) \tag{A.3}$$

$$F(\varphi)\frac{1}{\rho}\frac{\partial}{\partial\rho}\left(\rho\frac{\partial R(\rho)}{\partial\rho}\right) + R(\rho)\frac{1}{\rho^2}\frac{\partial^2 F(\varphi)}{\partial\varphi^2} = 0 \tag{A.4}$$

$$\frac{\rho}{R(\rho)}\frac{\partial}{\partial\rho}\left(\rho\frac{\partial R(\rho)}{\partial\rho}\right) + \frac{1}{F(\varphi)}\frac{\partial^2 F(\varphi)}{\partial\varphi^2} = 0 \tag{A.5}$$

We now introduce the two separation-of-variables eigenvalues k_ρ^2 and k_φ^2 such that the independent terms for each variable in Eq.A.5 could be separated into two separate eigenvalue equations. These two eigenvalue equations, along with the relationship between the separation-of-variables eigenvalues, are listed below:

$$\left.\begin{aligned} &\frac{\rho}{R(\rho)}\frac{\partial}{\partial\rho}\left(\rho\frac{\partial R(\rho)}{\partial\rho}\right) = -k_\rho^2 \\ &\frac{1}{F(\varphi)}\frac{\partial^2 F(\varphi)}{\partial\varphi^2} = -k_\varphi^2 \\ &k_\rho^2 + k_\varphi^2 = 0 \end{aligned}\right\} \tag{A.6}$$

Given the azimuthal symmetry of the cylindrical geometry, we obtain the following periodic eigenvalue problem and condition for $F(\varphi)$:

$$\left.\begin{aligned} &\frac{\partial^2 F(\varphi)}{\partial\varphi^2} + k_\varphi^2 F(\varphi) = 0 \\ &F(\varphi + 2\pi) = F(\varphi) \end{aligned}\right\} \tag{A.7}$$

The resulting general solution for $F(\varphi)$ is expressed as follows:

$$F(\varphi) = A\sin(k_\varphi\varphi) + B\cos(k_\varphi\varphi) \tag{A.8}$$

The above expression for $F(\varphi)$ is a linear combination of two solutions to the periodic eigenvalue problem. Thus, it suffices to choose only one of the trigonometric functions as our solution without a loss of generality. However, since we are working with TEM modes, we know that $\phi(\rho, \varphi)$ is φ-invariant. This implies that $k_\varphi = 0$, which in turn means that $k_\rho = 0$ since $k_\rho^2 + k_\varphi^2 = 0$. Therefore, we choose a cosinusoidal varying function description as our only non-trivial solution to the periodic eigenvalue problem, which results with $F(\varphi) = B\cos(k_\varphi\varphi) = B$ when $k_\varphi \to 0$.

We now obtain the following eigenvalue problem and boundary conditions for $R(\rho)$:

$$\left.\begin{aligned} &\frac{\rho}{R(\rho)}\frac{\partial}{\partial\rho}\left(\rho\frac{\partial R(\rho)}{\partial\rho}\right)=0\\ &R(\rho=r_i)=V_0\\ &R(\rho=r_o)=0 \end{aligned}\right\} \tag{A.9}$$

The resulting general solution for $R(\rho)$ becomes:

$$R(\rho)=C\ln\rho+D \tag{A.10}$$

By implementing the boundary conditions from Eq.A.9 to determine the constants $\{C,D\}$ in Eq.A.10, the final solution for $R(\rho)$ becomes:

$$R(\rho)=V_0\ln\left(\frac{r_o}{r_i}\right)^{-1}\ln\left(\frac{r_o}{\rho}\right) \tag{A.11}$$

We could now express the final eigenfunction $\phi_0(\boldsymbol{\rho})=\phi_0(\rho,\varphi)$ as follows:

$$\begin{aligned}\phi_0(\rho,\varphi)&=R(\rho)F(\varphi)\\&=V_0\ln\left(\frac{r_o}{r_i}\right)^{-1}\ln\left(\frac{r_o}{\rho}\right)\end{aligned} \tag{A.12}$$

Here, the constant B from $F(\varphi)$ is accounted for in the arbitrary potential V_0. The transversal electric and magnetic field expansion functions $\mathbf{e}_0^{\mathrm{D}}(\boldsymbol{\rho})=\mathbf{e}_0^{\mathrm{D}}(\rho,\varphi)$ and $\mathbf{h}_0^{\mathrm{D}}(\boldsymbol{\rho})=\mathbf{h}_0^{\mathrm{D}}(\rho,\varphi)$ could now be expressed as follows:

$$\begin{aligned}\mathbf{e}_0^{\mathrm{D}}(\boldsymbol{\rho})&=\nabla_t\phi_0(\boldsymbol{\rho})\\&=\left(\frac{\partial}{\partial\rho}\hat{\boldsymbol{\rho}}+\frac{1}{\rho}\frac{\partial}{\partial\varphi}\hat{\boldsymbol{\varphi}}\right)\phi_0(\boldsymbol{\rho})\\&=\hat{\boldsymbol{\rho}}V_0\ln\left(\frac{r_o}{r_i}\right)^{-1}\frac{1}{\rho}\end{aligned} \tag{A.13}$$

$$\begin{aligned}\mathbf{h}_0^{\mathrm{D}}(\boldsymbol{\rho})&=\hat{\mathbf{z}}\times\nabla_t\phi_0(\boldsymbol{\rho})\\&=\left(\frac{\partial}{\partial\rho}\hat{\boldsymbol{\varphi}}-\frac{1}{\rho}\frac{\partial}{\partial\varphi}\hat{\boldsymbol{\rho}}\right)\phi_0(\boldsymbol{\rho})\\&=\hat{\boldsymbol{\varphi}}V_0\ln\left(\frac{r_o}{r_i}\right)^{-1}\frac{1}{\rho}\end{aligned} \tag{A.14}$$

In Eq.A.13 and Eq.A.14, a minus sign originating from the above analytical derivations has been absorbed by the arbitrary potential constant V_0. We could now obtain the unnormalized TEM field expressions by appending the following excitation functions $u_0^{\mathrm{D}}(z,t)$ and $i_0^{\mathrm{D}}(z,t)$ as follows:

$$\mathbf{E}_t(\mathbf{r},t)=u_0^{\mathrm{D}}(z,t)\mathbf{e}_0^{\mathrm{D}}(\boldsymbol{\rho}) \tag{A.15}$$

$$\mathbf{H}_t(\mathbf{r},t)=i_0^{\mathrm{D}}(z,t)\mathbf{h}_0^{\mathrm{D}}(\boldsymbol{\rho}) \tag{A.16}$$

We proceed by expressing the source-free free-space excitation problem in both the time and frequency domain, where the conversion between the two domains has been achieved using the $j\omega$-method:

Time-domain formulation:

$$\left.\begin{aligned} &\frac{\partial u_0^{\mathrm{D}}(z,t)}{\partial z}+\mu_0\frac{\partial i_0^{\mathrm{D}}(z,t)}{\partial t}=0\\ &\frac{\partial i_0^{\mathrm{D}}(z,t)}{\partial z}+\varepsilon_0\frac{\partial u_0^{\mathrm{D}}(z,t)}{\partial t}=0 \end{aligned}\right\} \tag{A.17}$$

Frequency-domain formulation:

$$\left.\begin{aligned}\frac{\partial U_0^{\mathrm{D}}(z,\omega)}{\partial z}+j\omega\mu_0 I_0^{\mathrm{D}}(z,\omega)=0\\ \frac{\partial I_0^{\mathrm{D}}(z,\omega)}{\partial z}+j\omega\varepsilon_0 U_0^{\mathrm{D}}(z,\omega)=0\end{aligned}\right\} \tag{A.18}$$

For simplicity, we assume one operating frequency and proceed with solving the frequency-domain formulation as a system of equations:

$$\left.\begin{aligned}\frac{\partial^2 U_0^{\mathrm{D}}(z)}{\partial z^2}+k^2 U_0^{\mathrm{D}}(z)=0\\ \frac{\partial U_0^{\mathrm{D}}(z)}{\partial z}+j\omega\mu_0 I_0^{\mathrm{D}}(z)=0\end{aligned}\right\} \tag{A.19}$$

The aforementioned system of equations yields the following solution for each excitation function:

$$U_0^{\mathrm{D}}(z)=a_0^{\mathrm{D}+}e^{-jkz}+a_0^{\mathrm{D}-}e^{+jkz} \tag{A.20}$$

$$I_0^{\mathrm{D}}(z)=\frac{1}{\eta}\left(a_0^{\mathrm{D}+}e^{-jkz}-a_0^{\mathrm{D}-}e^{+jkz}\right) \tag{A.21}$$

Here we have introduced the free-space wave number $k=\omega^2\mu_0\varepsilon_0$, the free-space wave impedance $\eta=\sqrt{\mu_0/\varepsilon_0}$, and the undetermined excitation coefficients $a_0^{\mathrm{D}\pm}$. The normalized TEM field expression is now obtained as follows:

$$\boldsymbol{E}^{\mathrm{TEM}}(\mathbf{r})=a_0^{\mathrm{D}+}e^{-jkz}\boldsymbol{E}_0^{\mathrm{D}+}(\boldsymbol{\rho})+a_0^{\mathrm{D}-}e^{+jkz}\boldsymbol{E}_0^{\mathrm{D}-}(\boldsymbol{\rho}) \tag{A.22}$$

$$\boldsymbol{H}^{\mathrm{TEM}}(\mathbf{r})=a_0^{\mathrm{D}+}e^{-jkz}\boldsymbol{H}_0^{\mathrm{D}+}(\boldsymbol{\rho})+a_0^{\mathrm{D}-}e^{+jkz}\boldsymbol{H}_0^{\mathrm{D}-}(\boldsymbol{\rho}) \tag{A.23}$$

Where the modal fields are re-expressed as follows:

$$\boldsymbol{E}_0^{\mathrm{D}\pm}(\boldsymbol{\rho})=\boldsymbol{e}_0^{\mathrm{D}}(\boldsymbol{\rho}) \tag{A.24}$$

$$\boldsymbol{H}_0^{\mathrm{D}\pm}(\boldsymbol{\rho})=\pm\frac{1}{\eta}\boldsymbol{h}_0^{\mathrm{D}}(\boldsymbol{\rho}) \tag{A.25}$$

As a normalization condition, we require the modal fields to transport one unit of apparent power

along the waveguide cross-section:

$$
\begin{aligned}
\left|\frac{1}{2}\int_A \left(\boldsymbol{E}_0^{\mathrm{D}\pm}\times\boldsymbol{H}_0^{\mathrm{D}\pm}\right)\cdot\hat{\mathbf{z}}ds\right| &= \left|\frac{1}{2}\int_0^{2\pi}\int_{r_i}^{r_o}\left(\boldsymbol{E}_0^{\mathrm{D}\pm}\times\boldsymbol{H}_0^{\mathrm{D}\pm}\right)\cdot\hat{\mathbf{z}}\rho d\rho d\varphi\right| \\
&= \left|\frac{1}{2}\int_0^{2\pi}\int_{r_i}^{r_o}\left(\boldsymbol{e}_0^{\mathrm{D}}(\boldsymbol{\rho})\times\pm\frac{1}{\eta}\boldsymbol{h}_0^{\mathrm{D}}(\boldsymbol{\rho})\right)\cdot\hat{\mathbf{z}}\rho d\rho d\varphi\right| \\
&= \left|\frac{1}{2\eta}\int_0^{2\pi}\int_{r_i}^{r_o}\left(\boldsymbol{e}_0^{\mathrm{D}}(\boldsymbol{\rho})\times\pm\left[\hat{\mathbf{z}}\times\mathbf{e}_0^{\mathrm{D}}(\boldsymbol{\rho})\right]\right)\cdot\hat{\mathbf{z}}\rho d\rho d\varphi\right| \\
&= \{\hat{\mathbf{a}}\times(\hat{\mathbf{b}}\times\hat{\mathbf{c}}) = \hat{\mathbf{b}}(\hat{\mathbf{a}}\cdot\hat{\mathbf{c}}) - \hat{\mathbf{c}}(\hat{\mathbf{a}}\cdot\hat{\mathbf{b}}),\ \hat{\mathbf{z}}\cdot\boldsymbol{e}_0^{\mathrm{D}}(\boldsymbol{\rho}) = 0\} \\
&= \frac{1}{2\eta}\int_0^{2\pi}\int_{r_i}^{r_o}\left|\boldsymbol{e}_0^{\mathrm{D}}(\boldsymbol{\rho})\right|^2\rho d\rho d\varphi \\
&= \frac{1}{2\eta}\int_0^{2\pi}\int_{r_i}^{r_o}\left|V_0\left(\ln\frac{r_o}{r_i}\right)^{-1}\frac{1}{\rho}\right|^2\rho d\rho d\varphi \\
&= \frac{V_0^2}{2\eta\ln\left(\frac{r_o}{r_i}\right)^2}\int_0^{2\pi}\int_{r_i}^{r_o}\frac{1}{\rho}d\rho d\varphi \\
&= \frac{2\pi V_0^2}{2\eta\ln\left(\frac{r_o}{r_i}\right)^2}\left[\ln|\rho|\right]_{r_i}^{r_o} \\
&= \frac{\pi V_0^2}{\eta\ln\left(\frac{r_o}{r_i}\right)} \\
&= D_0^2 \\
&= 1
\end{aligned}
\tag{A.26}
$$

Here we define the normalization constant D_0 as follows:

$$
D_0 = V_0\sqrt{\frac{\pi}{\eta\ln\left(\frac{r_o}{r_i}\right)}} \tag{A.27}
$$

The power normalized modal field could now be explicitly expressed as follows:

$$
\begin{aligned}
\boldsymbol{E}_0^{\mathrm{D}\pm}(\boldsymbol{\rho}) &= \frac{1}{D_0}\boldsymbol{e}_0^{\mathrm{D}}(\boldsymbol{\rho}) \\
&= \frac{1}{D_0}\nabla_t\phi_0(\boldsymbol{\rho}) \\
&= \hat{\boldsymbol{\rho}}\sqrt{\frac{\eta}{\pi\ln\left(\frac{r_o}{r_i}\right)}}\frac{1}{\rho}
\end{aligned}
\tag{A.28}
$$

$$
\begin{aligned}
\boldsymbol{H}_0^{\mathrm{D}\pm}(\boldsymbol{\rho}) &= \pm\frac{1}{\eta D_0}\boldsymbol{h}_0^{\mathrm{D}}(\boldsymbol{\rho}) \\
&= \pm\frac{1}{\eta D_0}\hat{\mathbf{z}}\times\nabla_t\phi_0(\boldsymbol{\rho}) \\
&= \pm\hat{\boldsymbol{\varphi}}\sqrt{\frac{1}{\pi\eta\ln\left(\frac{r_o}{r_i}\right)}}\frac{1}{\rho}
\end{aligned}
\tag{A.29}
$$

The complete power normalized frequency domain electric and magnetic field expressions could now be expressed using Eq.A.22, Eq.A.23, Eq.A.28 and Eq.A.29.

Appendix B Derive analytical expressions for the TM-modes in a circular waveguide.

We proceed to derive the analytical expressions for the electric and magnetic fields of TM-modes in a circular waveguide using an eigenvalue problem description. The Dirichlet boundary problem, using eigenfunction $\phi(\boldsymbol{\rho}) = \phi(\rho, \varphi)$ and the transversal eigenvalue d_t, for TM modes in a circular waveguide is expressed as follows:

$$\left.\begin{aligned} &\left(\nabla_t^2 + d_t^2\right)\phi(\rho,\varphi) = 0 \\ &\phi(\rho = r_o, \varphi) = 0 \end{aligned}\right\} \tag{B.1}$$

Here we have that r_o represents the circular waveguide radius. We start by expressing the Helmholtz equation explicitly in cylindrical coordinates:

$$\left(\frac{1}{\rho}\frac{\partial}{\partial\rho}\left(\rho\frac{\partial}{\partial\rho}\right) + \frac{1}{\rho^2}\frac{\partial^2}{\partial\varphi^2} + d_t^2\right)\phi(\rho,\varphi) = 0 \tag{B.2}$$

We could solve the Helmholtz equation by using the method of separation of variables. After an appropriate separation ansatz has been chosen and introduced it into Eq.B.2, the resulting expression is then divided by the separation ansatz and multiplied by ρ^2. This is done so that we achieve independent terms for each variable in Eq.B.2.

$$\phi(\rho,\varphi) = R(\rho)F(\varphi) \tag{B.3}$$

$$F(\varphi)\frac{1}{\rho}\frac{\partial}{\partial\rho}\left(\rho\frac{\partial R(\rho)}{\partial\rho}\right) + R(\rho)\frac{1}{\rho^2}\frac{\partial^2 F(\varphi)}{\partial\varphi^2} + d_t^2 R(\rho)F(\varphi) = 0 \tag{B.4}$$

$$\frac{\rho}{R(\rho)}\frac{\partial}{\partial\rho}\left(\rho\frac{\partial R(\rho)}{\partial\rho}\right) + \frac{1}{F(\varphi)}\frac{\partial^2 F(\varphi)}{\partial\varphi^2} + d_t^2\rho^2 = 0 \tag{B.5}$$

We now introduce the two separation-of-variables eigenvalues k_ρ^2 and k_φ^2 such that the independent terms for each variable in Eq.B.5 could be separated into two separate eigenvalue equations. These two eigenvalue equations, along with the relationship between the separation-of-variables eigenvalues, are listed below:

$$\left.\begin{aligned} &\frac{\rho}{R(\rho)}\frac{\partial}{\partial\rho}\left(\rho\frac{\partial R(\rho)}{\partial\rho}\right) + d_t^2\rho^2 = -k_\rho^2 \\ &\frac{1}{F(\varphi)}\frac{\partial^2 F(\varphi)}{\partial\varphi^2} = -k_\varphi^2 \\ &k_\rho^2 + k_\varphi^2 = 0 \end{aligned}\right\} \tag{B.6}$$

Here we chose to insert the Dirichlet eigenvalue into the polar eigenvalue equation. Given the azimuthal symmetry of the cylindrical geometry, we obtain the following periodic eigenvalue problem and condition for $F(\varphi)$:

$$\left.\begin{aligned} &\frac{\partial^2 F(\varphi)}{\partial\varphi^2} + k_\varphi^2 F(\varphi) = 0 \\ &F(\varphi + 2\pi) = F(\varphi) \end{aligned}\right\} \tag{B.7}$$

The resulting general solution for $F(\varphi)$ is expressed as follows:

$$F(\varphi) = A\sin\left(k_\varphi\varphi\right) + B\cos\left(k_\varphi\varphi\right) \tag{B.8}$$

The above expression for $F(\varphi)$ is a linear combination of two solutions to the periodic eigenvalue problem. Thus, it suffices to choose only one of the trigonometric functions as our solution without a loss of generality. The aforementioned periodic boundary condition implies that $k_\varphi = m$ where $m \subset \mathbb{Z}^+$, which in turn means that $k_\rho^2 = -k_\varphi^2 = -m^2$ since $k_\rho^2 + k_\varphi^2 = 0$. Therefore, we choose a cosinusoidal varying function description as our only non-trivial solution to the periodic eigenvalue problem, which results with $F(\varphi) = B\cos\left(k_\varphi\varphi\right)$ for all $m \subset \mathbb{Z}^+$. The non-triviality of $F(\varphi)$ for when $m = 0$ will be important during the orthogonalization process of the eigenfunction later on.

We now obtain the following eigenvalue problem and boundary conditions for $R(\rho)$:

$$\left.\begin{aligned} &\rho\frac{\partial}{\partial\rho}\left(\rho\frac{\partial R(\rho)}{\partial\rho}\right)+\left(d_t^2\rho^2-m^2\right)R(\rho)=0\\ &R(\rho=r_o)=0 \end{aligned}\right\} \tag{B.9}$$

The above eigenvalue problem represents the Bessel differential equation and the resulting general solution for $R(\rho)$ becomes:

$$R(\rho)=CJ_m\left(d_t\rho\right)+DY_m\left(d_t\rho\right) \tag{B.10}$$

The above expression for $R(\rho)$ consists of the first and second-order Bessel function $\{J_m\left(d_t\rho\right),Y_m\left(d_t\rho\right)\}$ respectively, and is a linear combination of two functions to the Bessel differential equation. However, since we are considering a circular waveguide, the second-order Bessel function $Y_m\left(d_t\rho\right)$ will diverge to infinity as $\rho_{min}\to 0$. In order to maintain a realistic nature of the field solution inside the circular waveguide, we choose that $D=0$. Thus, it suffices to choose only the first-order Bessel function $J_m\left(d_t\rho\right)$ as our solution without a loss of generality. Finally, we implement the boundary condition from Eq.B.9, which results with $R(\rho)=CJ_m\left(d_{tmn}\rho\right)$ where $d_{tmn}=\xi_{mn}/r_o$. Here ξ_{mn} represents the nth zero of the mth order Bessel function of the first kind where $m\subset\mathbb{Z}^+$ and $n\subset\mathbb{N}$.

We could now express the final eigenfunction $\phi(\boldsymbol{\rho})=\phi_{mn}(\rho,\varphi)$ as follows:

$$\begin{aligned} \phi_{mn}(\rho,\varphi)&=R(\rho)F(\varphi)\\ &=C\cos\left(k_\varphi\varphi\right)J_m\left(d_{tmn}\rho\right)\\ &=C\cos\left(m\varphi\right)J_m\left(\xi_{mn}\frac{\rho}{r_o}\right) \end{aligned} \tag{B.11}$$

Here, the constant B from $F(\varphi)$ is accounted for in the constant C above. We proceed by performing an orthogonalization procedure on the eigenfunction in Eq.B.11 using the orthogonality relation Eq.5.14a from the Compendium. This procedure is relevant for us since the orthogonality relation for the eigenvalue functions is inherited by the transversal field expansion functions, which is shown in Eq.5.67a from the Compendium. This is a valuable property that will be exploited during the power normalization procedure of the modal fields further on. Both the transversal field expansion functions and the modal fields will be defined later on. Before we perform the orthogonalization procedure, we acknowledge the following two integral solutions:

$$\begin{aligned} \int_0^{2\pi}\cos^2\left(m\varphi\right)d\varphi&=\left[\frac{\varphi}{2}+\frac{\sin\left(2m\varphi\right)}{4m}\right]_0^{2\pi}\\ &=\left(1+\delta_{m,0}\right)\pi \end{aligned} \tag{B.12}$$

$$\begin{aligned} \int_0^{r_o}\rho J_m^2\left(\xi_{mn}\frac{\rho}{r_o}\right)d\rho&=\frac{1}{2}\left[\rho^2J_m'^2\left(\xi_{mn}\frac{\rho}{r_o}\right)+\left(\rho^2-\frac{m^2r_o^2}{\xi_{mn}^2}\right)J_m^2\left(\xi_{mn}\frac{\rho}{r_o}\right)\right]_0^{r_o}\\ &=\frac{r_o^2}{2}J_m'^2\left(\xi_{mn}\right)+\frac{m^2r_o^2}{2\xi_{mn}^2}J_m^2\left(0\right)\\ &=\frac{r_o^2}{2}J_m'^2\left(\xi_{mn}\right)\\ &=\frac{r_o^2}{2}J_{m+1}^2\left(\xi_{mn}\right) \end{aligned} \tag{B.13}$$

Even though $J_m^2\left(0\right)\neq 0$ only when $m=0$, the second term in Eq.B.13 becomes zero since the multiplicative fractional term has a factor m^2 in the denominator. Here we have made use of the recurrence relation $\{J_m'\left(x\right)=\left(m/x\right)J_m\left(x\right)-J_{m+1}\left(x\right)\}$ along with the boundary conditions for the Bessel function, which results with $\left\{J_m'^2\left(x\right)=J_{m+1}^2\left(x\right)\right\}$. Moving forward, we will use $\{J_m'\left(x\right)=J_{m+1}\left(x\right)\}$ in order to avoid the derivative of the Bessel function. By using the integral results presented in Eq.B.12

and Eq.B.13, the orthogonalization procedure of the eigenfunction results with the following expression:

$$\begin{aligned}\int_A \phi_{kl}(\rho,\varphi)\phi_{mn}(\rho,\varphi)ds &= \delta_{km}\delta_{ln}\int_A \phi_{mn}^2(\rho,\varphi)ds \\ &= \delta_{km}\delta_{ln}\int_0^{2\pi}\int_0^{r_o} C^2\cos^2(m\varphi)J_m^2\left(\xi_{mn}\frac{\rho}{r_o}\right)\rho d\rho d\varphi \\ &= \delta_{km}\delta_{ln}C^2\int_0^{2\pi}\cos^2(m\varphi)d\varphi\int_0^{r_o}\rho J_m^2\left(\xi_{mn}\frac{\rho}{r_o}\right)d\rho \\ &= \delta_{km}\delta_{ln}C^2(1+\delta_{m,0})\,\pi\frac{r_o^2}{2}J_{m+1}^2(\xi_{mn}) \\ &= \delta_{km}\delta_{ln}D_{mn}^2\end{aligned} \tag{B.14}$$

Here we have exploited the orthogonality relation for the eigenfunctions, which is presented in Eq.5.14a from the Compendium. The constant C could now be expressed as follows:

$$\begin{aligned}C &= \sqrt{\frac{2}{(1+\delta_{m,0})\,\pi r_o^2 J_{m+1}^2(\xi_{mn})}}D_{mn} \\ &= \sqrt{\frac{(2-\delta_{m,0})}{\pi r_o^2 J_{m+1}^2(\xi_{mn})}}D_{mn} \\ &= \frac{\sqrt{(2-\delta_{m,0})}}{r_o\sqrt{\pi}J_{m+1}(\xi_{mn})}D_{mn}\end{aligned} \tag{B.15}$$

In Eq.B.15 we have introduced the normalization constant D_{mn}, which will be determined during the normalization procedure of the modal fields later on. We could now express the final orthogonalized eigenfunction $\phi_{mn}(\rho,\varphi)$ as follows:

$$\phi_{mn}(\rho,\varphi) = D_{mn}\frac{\sqrt{2-\delta_{m,0}}}{r_o\sqrt{\pi}J_{m+1}(\xi_{mn})}\cos(m\varphi)J_m\left(\xi_{mn}\frac{\rho}{r_o}\right) \tag{B.16}$$

The transversal electric and magnetic field expansion functions $\mathbf{e}_{mn}^{\mathrm{D}}(\boldsymbol{\rho}) = \mathbf{e}_{mn}^{\mathrm{D}}(\rho,\varphi)$ and $\mathbf{h}_{mn}^{\mathrm{D}}(\boldsymbol{\rho}) = \mathbf{h}_{mn}^{\mathrm{D}}(\rho,\varphi)$ could now be expressed as follows:

$$\begin{aligned}\mathbf{e}_{mn}^{\mathrm{D}}(\boldsymbol{\rho}) &= \nabla_t\phi_{mn}(\boldsymbol{\rho}) \\ &= \left(\frac{\partial}{\partial\rho}\hat{\boldsymbol{\rho}} + \frac{1}{\rho}\frac{\partial}{\partial\varphi}\hat{\boldsymbol{\varphi}}\right)\phi_{mn}(\boldsymbol{\rho}) \\ &= \hat{\boldsymbol{\rho}}\mathbf{e}_{\rho mn}^{\mathrm{D}}(\boldsymbol{\rho}) + \hat{\boldsymbol{\varphi}}\mathbf{e}_{\varphi mn}^{\mathrm{D}}(\boldsymbol{\rho}) \\ &= \hat{\boldsymbol{\rho}}D_{mn}\frac{\xi_{mn}}{r_o^2}\sqrt{\frac{2-\delta_{m,0}}{\pi}}\frac{J_m'\left(\xi_{mn}\frac{\rho}{r_o}\right)}{J_{m+1}(\xi_{mn})}\cos(m\varphi) \\ &\quad - \hat{\boldsymbol{\varphi}}D_{mn}\frac{m}{r_o\rho}\sqrt{\frac{2-\delta_{m,0}}{\pi}}\frac{J_m\left(\xi_{mn}\frac{\rho}{r_o}\right)}{J_{m+1}(\xi_{mn})}\sin(m\varphi) \\ &= \hat{\boldsymbol{\rho}}D_{mn}\frac{\xi_{mn}}{r_o^2}\sqrt{\frac{2-\delta_{m,0}}{\pi}}\frac{\left[\left(\frac{mr_o}{\xi_{mn}\rho}\right)J_m\left(\xi_{mn}\frac{\rho}{r_o}\right) - J_{m+1}\left(\xi_{mn}\frac{\rho}{r_o}\right)\right]}{J_{m+1}(\xi_{mn})}\cos(m\varphi) \\ &\quad - \hat{\boldsymbol{\varphi}}D_{mn}\frac{m}{r_o\rho}\sqrt{\frac{2-\delta_{m,0}}{\pi}}\frac{J_m\left(\xi_{mn}\frac{\rho}{r_o}\right)}{J_{m+1}(\xi_{mn})}\sin(m\varphi)\end{aligned} \tag{B.17}$$

$$
\begin{aligned}
\mathbf{h}^{\mathrm{D}}_{mn}(\boldsymbol{\rho}) &= \hat{\mathbf{z}} \times \nabla_t \phi_{mn}(\boldsymbol{\rho}) \\
&= \left(\frac{\partial}{\partial \rho} \hat{\boldsymbol{\varphi}} - \frac{1}{\rho} \frac{\partial}{\partial \varphi} \hat{\boldsymbol{\rho}} \right) \phi_{mn}(\boldsymbol{\rho}) \\
&= \hat{\boldsymbol{\varphi}} \mathbf{e}^{\mathrm{D}}_{\rho mn}(\boldsymbol{\rho}) - \hat{\boldsymbol{\rho}} \mathbf{e}^{\mathrm{D}}_{\varphi mn}(\boldsymbol{\rho}) \\
&= \hat{\boldsymbol{\rho}} D_{mn} \frac{m}{r_o \rho} \sqrt{\frac{2-\delta_{m,0}}{\pi}} \frac{J_m\left(\xi_{mn} \dfrac{\rho}{r_o}\right)}{J_{m+1}\left(\xi_{mn}\right)} \sin\left(m\varphi\right) \\
&\quad + \hat{\boldsymbol{\varphi}} D_{mn} \frac{\xi_{mn}}{r_o^2} \sqrt{\frac{2-\delta_{m,0}}{\pi}} \frac{J'_m\left(\xi_{mn} \dfrac{\rho}{r_o}\right)}{J_{m+1}\left(\xi_{mn}\right)} \cos\left(m\varphi\right) \\
&= \hat{\boldsymbol{\rho}} D_{mn} \frac{m}{r_o \rho} \sqrt{\frac{2-\delta_{m,0}}{\pi}} \frac{J_m\left(\xi_{mn} \dfrac{\rho}{r_o}\right)}{J_{m+1}\left(\xi_{mn}\right)} \sin\left(m\varphi\right) \\
&\quad + \hat{\boldsymbol{\varphi}} D_{mn} \frac{\xi_{mn}}{r_o^2} \sqrt{\frac{2-\delta_{m,0}}{\pi}} \frac{\left[\left(\dfrac{m r_o}{\xi_{mn}\rho}\right) J_m\left(\xi_{mn} \dfrac{\rho}{r_o}\right) - J_{m+1}\left(\xi_{mn} \dfrac{\rho}{r_o}\right)\right]}{J_{m+1}\left(\xi_{mn}\right)} \cos\left(m\varphi\right)
\end{aligned}
\tag{B.18}
$$

Continuing forward, we will denote $i = mn$ as a collective term for variable parameters, which is introduced for convenience. We could now obtain the unnormalized TM field expressions by appending the following excitation functions $u_i^{\mathrm{D}}(z,t)$, $i_i^{\mathrm{D}}(z,t)$, and $l_i^{\mathrm{D}}(z,t)$ and sum over all the excited modes as follows:

$$
\begin{aligned}
\mathbf{E}(\mathbf{r},t) &= \mathbf{E}_t(\mathbf{r},t) + \mathbf{E}_z(\mathbf{r},t) \\
&= \sum_{i=1}^{\infty} u_i^{\mathrm{D}}(z,t) \mathbf{e}_i^{\mathrm{D}}(\boldsymbol{\rho}) + \sum_{i=1}^{\infty} l_i^{\mathrm{D}}(z,t) \phi_i(\boldsymbol{\rho})
\end{aligned}
\tag{B.19}
$$

$$
\mathbf{H}_t(\mathbf{r},t) = \sum_{i=1}^{\infty} i_i^{\mathrm{D}}(z,t) \mathbf{h}_i^{\mathrm{D}}(\boldsymbol{\rho})
\tag{B.20}
$$

We proceed by expressing the source-free free-space TM excitation problem in both the time and frequency domain, where the conversion between the two domains has been achieved using the $j\omega$-method:

Time-domain formulation:

$$
\left.
\begin{aligned}
&\frac{\partial u_i^{\mathrm{D}}(z,t)}{\partial z} + \mu_0 \frac{\partial i_i^{\mathrm{D}}(z,t)}{\partial t} - l_i^{\mathrm{D}}(z,t) = 0 \\
&i_i^{\mathrm{D}}(z,t) + \frac{\varepsilon_0}{d_{ti}^2} \frac{\partial l_i^{\mathrm{D}}(z,t)}{\partial t} = 0 \\
&\frac{\partial i_i^{\mathrm{D}}(z,t)}{\partial z} + \varepsilon_0 \frac{\partial u_i^{\mathrm{D}}(z,t)}{\partial t} = 0
\end{aligned}
\right\}
\tag{B.21}
$$

Frequency-domain formulation:

$$
\left.
\begin{aligned}
&\frac{\partial U_i^{\mathrm{D}}(z,\omega)}{\partial z} + j\omega\mu_0 I_i^{\mathrm{D}}(z,\omega) - L_i^{\mathrm{D}}(z,\omega) = 0 \\
&I_i^{\mathrm{D}}(z,\omega) + j\omega \frac{\varepsilon_0}{d_{ti}^2} L_i^{\mathrm{D}}(z,\omega) = 0 \\
&\frac{\partial I_i^{\mathrm{D}}(z,\omega)}{\partial z} + j\omega\varepsilon_0 U_i^{\mathrm{D}}(z,\omega) = 0
\end{aligned}
\right\}
\tag{B.22}
$$

For simplicity, we assume one operating frequency and proceed with solving the frequency-domain formulation as a system of equations:

$$
\left.
\begin{aligned}
&\frac{\partial^2 U_i^{\mathrm{D}}(z)}{\partial z^2} + d_{zi}^2 U_i^{\mathrm{D}}(z) = 0 \\
&\frac{\partial U_i^{\mathrm{D}}(z)}{\partial z} + j \frac{\eta d_{zi}^2}{k} I_i^{\mathrm{D}}(z) = 0 \\
&I_i^{\mathrm{D}}(z) + j\omega \frac{\varepsilon_0}{d_{ti}^2} L_i^{\mathrm{D}}(z) = 0
\end{aligned}
\right\}
\tag{B.23}
$$

The aforementioned system of equations yields the following solution for each excitation function:

$$U_i^{\mathrm{D}}(z) = a_i^{\mathrm{D}+} e^{-jd_{zi}z} + a_i^{\mathrm{D}-} e^{+jd_{zi}z} \tag{B.24}$$

$$I_i^{\mathrm{D}}(z) = \frac{k}{\eta d_{zi}} \left(a_i^{\mathrm{D}+} e^{-jd_{zi}z} - a_i^{\mathrm{D}-} e^{+jd_{zi}z} \right) \tag{B.25}$$

$$L_i^{\mathrm{D}}(z) = \frac{jd_{ti}^2}{d_{zi}} \left(a_i^{\mathrm{D}+} e^{-jd_{zi}z} - a_i^{\mathrm{D}-} e^{+jd_{zi}z} \right) \tag{B.26}$$

Here we have introduced the free-space wave number $k = \omega^2 \mu_0 \varepsilon_0$, the free-space wave impedance $\eta = \sqrt{\mu_0/\varepsilon_0}$, the longitudinal eigenvalue $d_{zi} = \sqrt{k^2 - d_{ti}^2}$ where $\mathrm{Im}\{d_{zi}\} < 0$, and the undetermined excitation coefficients $a_i^{\mathrm{D}\pm}$. The normalized TM field expression is now obtained as follows:

$$\boldsymbol{E}^{\mathrm{TM}}(\mathbf{r}) = \sum_{i=1}^{\infty} \left[a_i^{\mathrm{D}+} e^{-jd_{zi}z} \boldsymbol{E}_i^{\mathrm{D}+}(\boldsymbol{\rho}) + a_i^{\mathrm{D}-} e^{+jd_{zi}z} \boldsymbol{E}_i^{\mathrm{D}-}(\boldsymbol{\rho}) \right] \tag{B.27}$$

$$\boldsymbol{H}^{\mathrm{TM}}(\mathbf{r}) = \sum_{i=1}^{\infty} \left[a_i^{\mathrm{D}+} e^{-jd_{zi}z} \boldsymbol{H}_i^{\mathrm{D}+}(\boldsymbol{\rho}) + a_i^{\mathrm{D}-} e^{+jd_{zi}z} \boldsymbol{H}_i^{\mathrm{D}-}(\boldsymbol{\rho}) \right] \tag{B.28}$$

Where the modal fields are re-expressed as follows:

$$\boldsymbol{E}_i^{\mathrm{D}\pm}(\boldsymbol{\rho}) = \boldsymbol{e}_i^{\mathrm{D}}(\boldsymbol{\rho}) \pm \frac{jd_{ti}^2}{d_{zi}} \phi_i(\boldsymbol{\rho}) \hat{\mathbf{z}} \tag{B.29}$$

$$\boldsymbol{H}_i^{\mathrm{D}\pm}(\boldsymbol{\rho}) = \pm \frac{k}{\eta d_{zi}} \boldsymbol{h}_i^{\mathrm{D}}(\boldsymbol{\rho}) \tag{B.30}$$

As a normalization condition, we require the modal fields to transport one unit of apparent power along the waveguide cross-section:

$$\begin{aligned}
\left| \frac{1}{2} \int_A \left(\boldsymbol{E}_i^{\mathrm{D}\pm} \times \boldsymbol{H}_i^{\mathrm{D}\pm} \right) \cdot \hat{\mathbf{z}} ds \right| &= \left| \frac{1}{2} \int_0^{2\pi} \int_0^{r_o} \left(\boldsymbol{E}_i^{\mathrm{D}\pm} \times \boldsymbol{H}_i^{\mathrm{D}\pm} \right) \cdot \hat{\mathbf{z}} \rho d\rho d\varphi \right| \\
&= \left| \frac{1}{2} \int_0^{2\pi} \int_0^{r_o} \left(\left[\boldsymbol{e}_i^{\mathrm{D}}(\boldsymbol{\rho}) \pm \frac{jd_{ti}^2}{d_{zi}} \phi_i(\boldsymbol{\rho}) \hat{\mathbf{z}} \right] \times \pm \frac{k}{\eta d_{zi}} \boldsymbol{h}_i^{\mathrm{D}}(\boldsymbol{\rho}) \right) \cdot \hat{\mathbf{z}} \rho d\rho d\varphi \right| \\
&= \left| \frac{1}{2} \int_0^{2\pi} \int_0^{r_o} \left(\boldsymbol{e}_i^{\mathrm{D}}(\boldsymbol{\rho}) \times \frac{k}{\eta d_{zi}} \boldsymbol{h}_i^{\mathrm{D}}(\boldsymbol{\rho}) \right) \cdot \hat{\mathbf{z}} \rho d\rho d\varphi \right| \\
&= \left| \frac{k}{2\eta d_{zi}} \int_0^{2\pi} \int_0^{r_o} \left(\boldsymbol{e}_i^{\mathrm{D}}(\boldsymbol{\rho}) \times \boldsymbol{h}_i^{\mathrm{D}}(\boldsymbol{\rho}) \right) \cdot \hat{\mathbf{z}} \rho d\rho d\varphi \right| \\
&= \left| \frac{k}{2\eta d_{zi}} d_{ti}^2 D_i^2 \right| \\
&= 1
\end{aligned} \tag{B.31}$$

Here we have exploited the inherited orthogonality relation for the transversal field expansion functions, which is presented in Eq.5.67a from the Compendium. The normalization constant D_i could be defined as follows:

$$D_i = \frac{1}{d_{ti}} \sqrt{\frac{2\eta \left| d_{zi} \right|}{k}} \tag{B.32}$$

By re-introducing the collective term $i = mn$, the power normalized modal field could now be explicitly

expressed as follows:

$$\begin{aligned}
\boldsymbol{E}_{mn}^{\mathrm{D}\pm}(\boldsymbol{\rho}) &= \boldsymbol{e}_{mn}^{\mathrm{D}}(\boldsymbol{\rho}) \pm \frac{j d_{tmn}^2}{d_{zmn}} \phi_{mn}(\boldsymbol{\rho}) \hat{\mathbf{z}} \\
&= \hat{\boldsymbol{\rho}} \frac{\xi_{mn}}{d_{tmn} r_o^2} \sqrt{\frac{2\eta \left| d_{zmn} \right| (2 - \delta_{m,0})}{k\pi}} \frac{\left[\left(\frac{m r_o}{\xi_{mn} \rho} \right) J_m \left(\xi_{mn} \frac{\rho}{r_o} \right) - J_{m+1} \left(\xi_{mn} \frac{\rho}{r_o} \right) \right]}{J_{m+1}(\xi_{mn})} \cos(m\varphi) \\
&\quad - \hat{\boldsymbol{\varphi}} \frac{m}{d_{tmn} r_o \rho} \sqrt{\frac{2\eta \left| d_{zmn} \right| (2 - \delta_{m,0})}{k\pi}} \frac{J_m \left(\xi_{mn} \frac{\rho}{r_o} \right)}{J_{m+1}(\xi_{mn})} \sin(m\varphi) \\
&\quad \pm \hat{\mathbf{z}} \frac{j d_{tmn}}{d_{zmn} r_o} \sqrt{\frac{2\eta \left| d_{zmn} \right| (2 - \delta_{m,0})}{k\pi}} \frac{J_m \left(\xi_{mn} \frac{\rho}{r_o} \right)}{J_{m+1}(\xi_{mn})} \cos(m\varphi)
\end{aligned} \tag{B.33}$$

$$\begin{aligned}
\boldsymbol{H}_{mn}^{\mathrm{D}\pm}(\boldsymbol{\rho}) &= \pm \frac{k}{\eta d_{zmn}} \boldsymbol{h}_{mn}^{\mathrm{D}}(\boldsymbol{\rho}) \\
&= \pm \hat{\boldsymbol{\rho}} \frac{m}{d_{tmn} d_{zmn} r_o \rho} \sqrt{\frac{2k \left| d_{zmn} \right| (2 - \delta_{m,0})}{\pi\eta}} \frac{J_m \left(\xi_{mn} \frac{\rho}{r_o} \right)}{J_{m+1}(\xi_{mn})} \sin(m\varphi) \\
&\quad \pm \hat{\boldsymbol{\varphi}} \frac{\xi_{mn}}{d_{tmn} d_{zmn} r_o^2} \sqrt{\frac{2k \left| d_{zmn} \right| (2 - \delta_{m,0})}{\pi\eta}} \frac{\left[\left(\frac{m r_o}{\xi_{mn} \rho} \right) J_m \left(\xi_{mn} \frac{\rho}{r_o} \right) - J_{m+1} \left(\xi_{mn} \frac{\rho}{r_o} \right) \right]}{J_{m+1}(\xi_{mn})} \cos(m\varphi)
\end{aligned} \tag{B.34}$$

The complete power normalized frequency domain electric and magnetic field expressions could now be expressed using Eq.B.27, Eq.B.28, Eq.B.33 and Eq.B.34.

Appendix C Derive analytical expressions for the TM-modes in a circular coaxial waveguide.

We proceed to derive the analytical expressions for the electric and magnetic field of TM-modes in a circular coaxial waveguide using an eigenvalue problem description. The Dirichlet boundary problem, using eigenfunction $\phi(\boldsymbol{\rho}) = \phi(\rho, \varphi)$ and the transversal eigenvalue d_t, for TM modes in a circular coaxial waveguide is expressed as follows:

$$\left.\begin{aligned} &\left(\nabla_t^2 + d_t^2\right)\phi(\rho,\varphi) = 0 \\ &\phi(\rho = r_o, \varphi) = 0 \\ &\phi(\rho = r_i, \varphi) = 0 \end{aligned}\right\} \tag{C.1}$$

Here we have that $\{r_o, r_i\}$ represent the outer and inner radius of the circular coaxial waveguide respectively. We start by expressing the Helmholtz equation explicitly in cylindrical coordinates:

$$\left(\frac{1}{\rho}\frac{\partial}{\partial\rho}\left(\rho\frac{\partial}{\partial\rho}\right) + \frac{1}{\rho^2}\frac{\partial^2}{\partial\varphi^2} + d_t^2\right)\phi(\rho,\varphi) = 0 \tag{C.2}$$

We could solve the Helmholtz equation by using the method of separation of variables. After an appropriate separation ansatz has been chosen and introduced it into Eq.C.2, the resulting expression is then divided by the separation ansatz and multiplied by ρ^2. This is done so that we achieve independent terms for each variable in Eq.C.2.

$$\phi(\rho,\varphi) = R(\rho)F(\varphi) \tag{C.3}$$

$$F(\varphi)\frac{1}{\rho}\frac{\partial}{\partial\rho}\left(\rho\frac{\partial R(\rho)}{\partial\rho}\right) + R(\rho)\frac{1}{\rho^2}\frac{\partial^2 F(\varphi)}{\partial\varphi^2} + d_t^2 R(\rho)F(\varphi) = 0 \tag{C.4}$$

$$\frac{\rho}{R(\rho)}\frac{\partial}{\partial\rho}\left(\rho\frac{\partial R(\rho)}{\partial\rho}\right) + \frac{1}{F(\varphi)}\frac{\partial^2 F(\varphi)}{\partial\varphi^2} + d_t^2\rho^2 = 0 \tag{C.5}$$

We now introduce the two separation-of-variables eigenvalues k_ρ^2 and k_φ^2 such that the independent terms for each variable in Eq.C.5 could be separated into two separate eigenvalue equations. These two eigenvalue equations, along with the relationship between the separation-of-variables eigenvalues, are listed below:

$$\left.\begin{aligned} &\frac{\rho}{R(\rho)}\frac{\partial}{\partial\rho}\left(\rho\frac{\partial R(\rho)}{\partial\rho}\right) + d_t^2\rho^2 = -k_\rho^2 \\ &\frac{1}{F(\varphi)}\frac{\partial^2 F(\varphi)}{\partial\varphi^2} = -k_\varphi^2 \\ &k_\rho^2 + k_\varphi^2 = 0 \end{aligned}\right\} \tag{C.6}$$

Here we chose to insert the Dirichlet eigenvalue into the polar eigenvalue equation. Given the azimuthal symmetry of the cylindrical geometry, we obtain the following periodic eigenvalue problem and condition for $F(\varphi)$:

$$\left.\begin{aligned} &\frac{\partial^2 F(\varphi)}{\partial\varphi^2} + k_\varphi^2 F(\varphi) = 0 \\ &F(\varphi + 2\pi) = F(\varphi) \end{aligned}\right\} \tag{C.7}$$

The resulting general solution for $F(\varphi)$ is expressed as follows:

$$F(\varphi) = A\sin(k_\varphi\varphi) + B\cos(k_\varphi\varphi) \tag{C.8}$$

The above expression for $F(\varphi)$ is a linear combination of two solutions to the periodic eigenvalue problem. Thus, it suffices to choose only one of the trigonometric functions as our solution without a loss of generality. The aforementioned periodic boundary condition implies that $k_\varphi = m$ where $m \subset \mathbb{Z}^+$, which in turn means that $k_\rho^2 = -k_\varphi^2 = -m^2$ since $k_\rho^2 + k_\varphi^2 = 0$. Therefore, we choose a cosinusoidal varying function description as our only non-trivial solution to the periodic eigenvalue problem, which results with $F(\varphi) = B\cos(k_\varphi\varphi)$ for all $m \subset \mathbb{Z}^+$. The non-triviality of $F(\varphi)$ for when $m = 0$ will be important during the orthogonalization process of the eigenfunction later on.

We now obtain the following eigenvalue problem and boundary conditions for $R(\rho)$:

$$\left.\begin{aligned} &\rho\frac{\partial}{\partial\rho}\left(\rho\frac{\partial R(\rho)}{\partial\rho}\right)+\left(d_t^2\rho^2-m^2\right)R(\rho)=0\\ &R(\rho=r_o)=0\\ &R(\rho=r_i)=0 \end{aligned}\right\} \tag{C.9}$$

The above eigenvalue problem represents the Bessel differential equation and the resulting general solution for $R(\rho)$ becomes:

$$R(\rho)=CJ_m\left(d_t\rho\right)+DY_m\left(d_t\rho\right) \tag{C.10}$$

The above expression for $R(\rho)$ consists of the first and second-order Bessel function $\{J_m\left(d_t\rho\right),Y_m\left(d_t\rho\right)\}$ respectively, and is a linear combination of two functions to the Bessel differential equation. Given that we are considering a circular coaxial waveguide, the second-order Bessel function $Y_m\left(d_t\rho\right)$ will not diverge to infinity as $\rho_{min}\to r_i>0$. By implementing the boundary condition from Eq.C.9, we get the following system of equations:

$$CJ_m\left(\xi_{mn}\frac{r_o}{r_i}\right)+DY_m\left(\xi_{mn}\frac{r_o}{r_i}\right)=0 \tag{C.11}$$

$$CJ_m\left(\xi_{mn}\right)+DY_m\left(\xi_{mn}\right)=0 \tag{C.12}$$

Here we have that $d_{tmn}=\xi_{mn}/r_i$, where ξ_{mn} represents the nth zero of the mth order Bessel-Neumann function in Eq.C.10. This system of equations represents a relationship between the first and second kind of Bessel functions at the boundary points and could be used for two unique tasks: (1) It could be used to eliminate one of the constants $\{C,D\}$; (2) It could be used to express a transcendental equation for determining either the nth zero of the mth order Bessel-Neumann function ξ_{mn} or the outer and inner radius $\{r_o,r_i\}$ of the circular coaxial waveguide respectively (depending on which of these quantities are considered known). These two tasks are going to be completed in the aforementioned order, starting with task (1) where we choose to eliminate constant D from Eq.C.10 by re-writing Eq.C.11 and Eq.C.12 as follows:

$$\begin{aligned} D=&-C\frac{J_m\left(\xi_{mn}\frac{r_o}{r_i}\right)}{Y_m\left(\xi_{mn}\frac{r_o}{r_i}\right)}\\ =&-C\frac{J_m\left(\xi_{mn}\right)}{Y_m\left(\xi_{mn}\right)} \end{aligned} \tag{C.13}$$

We proceed with task (2) and express a transcendental equation for determining either the nth zero of the mth order Bessel-Neumann function ξ_{mn} or the outer and inner radius $\{r_o,r_i\}$ of the circular coaxial waveguide. This equation is obtained by eliminating the constant C in Eq.C.13 and re-arranging the first and second kind Bessel functions as follows:

$$J_m\left(\xi_{mn}\right)Y_m\left(\xi_{mn}\frac{r_o}{r_i}\right)=J_m\left(\xi_{mn}\frac{r_o}{r_i}\right)Y_m\left(\xi_{mn}\right) \tag{C.14}$$

The resulting general solution for $R(\rho)$ now becomes:

$$\begin{aligned} R(\rho)&=CJ_m\left(\xi_{mn}\frac{\rho}{r_i}\right)+DY_m\left(\xi_{mn}\frac{\rho}{r_i}\right)\\ &=C\left[J_m\left(\xi_{mn}\frac{\rho}{r_i}\right)-\frac{J_m\left(\xi_{mn}\right)}{Y_m\left(\xi_{mn}\right)}Y_m\left(\xi_{mn}\frac{\rho}{r_i}\right)\right] \end{aligned} \tag{C.15}$$

Here we have made use of the inner boundary condition, Eq.C.12, to eliminate the constant D in Eq.C.15. We could now express the final eigenfunction $\phi(\boldsymbol{\rho})=\phi_{mn}(\rho,\varphi)$ as follows:

$$\begin{aligned} \phi_{mn}(\rho,\varphi)&=R(\rho)F(\varphi)\\ &=B\cos\left(k_\varphi\varphi\right)\left[CJ_m\left(d_t\rho\right)+DY_m\left(d_t\rho\right)\right]\\ &=C\cos\left(m\varphi\right)\left[J_m\left(\xi_{mn}\frac{\rho}{r_i}\right)-\frac{J_m\left(\xi_{mn}\right)}{Y_m\left(\xi_{mn}\right)}Y_m\left(\xi_{mn}\frac{\rho}{r_i}\right)\right] \end{aligned} \tag{C.16}$$

Here, the constant B from $F(\varphi)$ is accounted for in the constant C above. We proceed by performing an orthogonalization procedure on the eigenfunction in Eq.C.16 using the orthogonality relation Eq.5.14a from the Compendium. This procedure is relevant for us since the orthogonality relation for the eigenvalue functions is inherited by the transversal field expansion functions, which is shown in Eq.5.67a from the Compendium. This is a valuable property that will be exploited during the power normalization procedure of the modal fields further on. Both the transversal field expansion functions and the modal fields will be defined later on. Before we perform the orthogonalization procedure, we acknowledge the following integral solutions:

$$\begin{aligned}\int_0^{2\pi} \cos^2(m\varphi)d\varphi &= \left[\frac{\varphi}{2} + \frac{\sin(2m\varphi)}{4m}\right]_0^{2\pi} \\ &= (1+\delta_{m,0})\,\pi\end{aligned} \tag{C.17}$$

$$\begin{aligned}\int_{r_i}^{r_o} \rho J_m^2\left(\xi_{mn}\frac{\rho}{r_i}\right)d\rho &= \frac{1}{2}\left[\rho^2\left\{J_m^2\left(\xi_{mn}\frac{\rho}{r_i}\right) - J_{m-1}\left(\xi_{mn}\frac{\rho}{r_i}\right)J_{m+1}\left(\xi_{mn}\frac{\rho}{r_i}\right)\right\}\right]_{r_i}^{r_o} \\ &= \frac{r_o^2}{2}\left[J_m^2\left(\xi_{mn}\frac{r_o}{r_i}\right) - \frac{r_o^2}{2}J_{m-1}\left(\xi_{mn}\frac{r_o}{r_i}\right)J_{m+1}\left(\xi_{mn}\frac{r_o}{r_i}\right)\right] \\ &\quad - \frac{r_i^2}{2}\left[J_m^2(\xi_{mn}) - J_{m-1}(\xi_{mn})\,J_{m+1}(\xi_{mn})\right]\end{aligned} \tag{C.18}$$

$$\begin{aligned}\int_{r_i}^{r_o} \rho Y_m^2\left(\xi_{mn}\frac{\rho}{r_i}\right)d\rho &= \frac{1}{2}\left[\rho^2\left\{Y_m^2\left(\xi_{mn}\frac{\rho}{r_i}\right) - Y_{m-1}\left(\xi_{mn}\frac{\rho}{r_i}\right)Y_{m+1}\left(\xi_{mn}\frac{\rho}{r_i}\right)\right\}\right]_{r_i}^{r_o} \\ &= \frac{r_o^2}{2}\left[Y_m^2\left(\xi_{mn}\frac{r_o}{r_i}\right) - \frac{r_o^2}{2}Y_{m-1}\left(\xi_{mn}\frac{r_o}{r_i}\right)Y_{m+1}\left(\xi_{mn}\frac{r_o}{r_i}\right)\right] \\ &\quad - \frac{r_i^2}{2}\left[Y_m^2(\xi_{mn}) - Y_{m-1}(\xi_{mn})\,Y_{m+1}(\xi_{mn})\right]\end{aligned} \tag{C.19}$$

$$\begin{aligned}\int_{r_i}^{r_o} \rho J_m\left(\xi_{mn}\frac{\rho}{r_i}\right)Y_m\left(\xi_{mn}\frac{\rho}{r_i}\right)d\rho &= \frac{1}{2}\left[\rho^2\left\{J_m\left(\xi_{mn}\frac{\rho}{r_i}\right)Y_m\left(\xi_{mn}\frac{\rho}{r_i}\right) - J_{m-1}\left(\xi_{mn}\frac{\rho}{r_i}\right)Y_{m+1}\left(\xi_{mn}\frac{\rho}{r_i}\right)\right.\right. \\ &\quad \left.\left. - J_{m+1}\left(\xi_{mn}\frac{\rho}{r_i}\right)Y_{m-1}\left(\xi_{mn}\frac{\rho}{r_i}\right)\right\}\right]_{r_i}^{r_o} \\ &= \frac{r_o^2}{2}\left[J_m\left(\xi_{mn}\frac{r_o}{r_i}\right)Y_m\left(\xi_{mn}\frac{r_o}{r_i}\right) - J_{m-1}\left(\xi_{mn}\frac{r_o}{r_i}\right)Y_{m+1}\left(\xi_{mn}\frac{r_o}{r_i}\right)\right. \\ &\quad \left. - J_{m+1}\left(\xi_{mn}\frac{r_o}{r_i}\right)Y_{m-1}\left(\xi_{mn}\frac{r_o}{r_i}\right)\right] \\ &\quad - \frac{r_i^2}{2}\left[J_m(\xi_{mn})\,Y_m(\xi_{mn}) - J_{m-1}(\xi_{mn})\,Y_{m+1}(\xi_{mn})\right. \\ &\quad \left. - J_{m+1}(\xi_{mn})\,Y_{m-1}(\xi_{mn})\right]\end{aligned} \tag{C.20}$$

$$
\begin{aligned}
&\int_{r_i}^{r_o} \rho \left[J_m\left(\xi_{mn}\frac{\rho}{r_i}\right) - \frac{J_m\left(\xi_{mn}\right)}{Y_m\left(\xi_{mn}\right)} Y_m\left(\xi_{mn}\frac{\rho}{r_i}\right)\right]^2 d\rho \\
&= \int_{r_i}^{r_o} \rho J_m^2\left(\xi_{mn}\frac{\rho}{r_i}\right) d\rho + \frac{J_m^2\left(\xi_{mn}\right)}{Y_m^2\left(\xi_{mn}\right)} \int_{r_i}^{r_o} \rho Y_m^2\left(\xi_{mn}\frac{\rho}{r_i}\right) d\rho - 2\frac{J_m\left(\xi_{mn}\right)}{Y_m\left(\xi_{mn}\right)} \int_{r_i}^{r_o} \rho J_m\left(\xi_{mn}\frac{\rho}{r_i}\right) Y_m\left(\xi_{mn}\frac{\rho}{r_i}\right) d\rho \\
&= \frac{1}{2}\left[\rho^2 \left\{ -J_{m-1}\left(\xi_{mn}\frac{\rho}{r_i}\right) J_{m+1}\left(\xi_{mn}\frac{\rho}{r_i}\right) - \frac{J_m^2\left(\xi_{mn}\right)}{Y_m^2\left(\xi_{mn}\right)} Y_{m-1}\left(\xi_{mn}\frac{\rho}{r_i}\right) Y_{m+1}\left(\xi_{mn}\frac{\rho}{r_i}\right) \right.\right. \\
&\quad \left.\left. + \frac{J_m\left(\xi_{mn}\right)}{Y_m\left(\xi_{mn}\right)} J_{m-1}\left(\xi_{mn}\frac{\rho}{r_i}\right) Y_{m+1}\left(\xi_{mn}\frac{\rho}{r_i}\right) + \frac{J_m\left(\xi_{mn}\right)}{Y_m\left(\xi_{mn}\right)} J_{m+1}\left(\xi_{mn}\frac{\rho}{r_i}\right) Y_{m-1}\left(\xi_{mn}\frac{\rho}{r_i}\right) \right\}\right]_{r_i}^{r_o} \\
&= -\frac{1}{2}\left[\rho^2 \left\{ \left(J_{m-1}\left(\xi_{mn}\frac{\rho}{r_i}\right) - \frac{J_m\left(\xi_{mn}\right)}{Y_m\left(\xi_{mn}\right)} Y_{m-1}\left(\xi_{mn}\frac{\rho}{r_i}\right)\right) \times \left(J_{m+1}\left(\xi_{mn}\frac{\rho}{r_i}\right) - \frac{J_m\left(\xi_{mn}\right)}{Y_m\left(\xi_{mn}\right)} Y_{m+1}\left(\xi_{mn}\frac{\rho}{r_i}\right)\right) \right\}\right]_{r_i}^{r_o} \\
&= -\frac{1}{2}\left[\rho^2 L_{m-1}\left(\xi_{mn}\frac{\rho}{r_i}\right) L_{m+1}\left(\xi_{mn}\frac{\rho}{r_i}\right)\right]_{r_i}^{r_o} \\
&= \frac{1}{2}\left[r_i^2 L_{m-1}\left(\xi_{mn}\right) L_{m+1}\left(\xi_{mn}\right) - r_o^2 L_{m-1}\left(\xi_{mn}\frac{r_o}{r_i}\right) L_{m+1}\left(\xi_{mn}\frac{r_o}{r_i}\right)\right]
\end{aligned}
\tag{C.21}
$$

For the last integral, Eq.C.21, we have introduced the following definition:

$$
L_\nu\left(\xi_{mn}\frac{\rho}{r_i}\right) = J_\nu\left(\xi_{mn}\frac{\rho}{r_i}\right) - \frac{J_m\left(\xi_{mn}\right)}{Y_m\left(\xi_{mn}\right)} Y_\nu\left(\xi_{mn}\frac{\rho}{r_i}\right) \tag{C.22}
$$

We obtain the resulting expression for Eq.C.21 by exploiting the integral solutions from Eq.C.18, Eq.C.19, and Eq.C.20, along with using the boundary relation $\left\{ L_\nu^2\left(\xi_{mn}\frac{\rho}{r_i}\right) \to 0 \right\}$ for $\{\rho = r_o, r_i\}$. Given that Eq.C.22 represents a superposition of the first and second kind Bessel functions, the recurrence relations are all applicable. Moving forward, we will use $\{L'_\nu(x) = (\nu/x) L_\nu(x) - L_{\nu+1}(x)\}$ in order to avoid the derivative of Bessel functions and express the following results using Eq.C.22 instead of $R(\rho)$ for convenience. By using the integral results presented in Eq.C.17 and Eq.C.21, the orthogonalization procedure of the eigenfunction results with the following expression:

$$
\begin{aligned}
\int_A \phi_{kl}(\rho,\varphi)\phi_{mn}(\rho,\varphi) ds &= \delta_{km}\delta_{ln} \int_A \phi_{mn}^2(\rho,\varphi) ds \\
&= \delta_{km}\delta_{ln} \int_0^{2\pi} \int_{r_i}^{r_o} C^2 \cos^2(m\varphi) L_m^2\left(\xi_{mn}\frac{\rho}{r_i}\right) \rho d\rho d\varphi \\
&= \delta_{km}\delta_{ln} C^2 \int_0^{2\pi} \cos^2(m\varphi) d\varphi \int_{r_i}^{r_o} \rho L_m^2\left(\xi_{mn}\frac{\rho}{r_i}\right) d\rho \\
&= \delta_{km}\delta_{ln} C^2 (1+\delta_{m,0})\pi \frac{1}{2}\left[r_i^2 L_{m-1}\left(\xi_{mn}\right) L_{m+1}\left(\xi_{mn}\right) - r_o^2 L_{m-1}\left(\xi_{mn}\frac{r_o}{r_i}\right) L_{m+1}\left(\xi_{mn}\frac{r_o}{r_i}\right)\right] \\
&= \delta_{km}\delta_{ln} D_{mn}^2
\end{aligned}
\tag{C.23}
$$

Here we have exploited the orthogonality relation for the eigenfunctions, which is presented in Eq.5.14a from the Compendium. The constant C could now be expressed as follows:

$$
\begin{aligned}
C &= \sqrt{\frac{2}{(1+\delta_{m,0})\pi\left[r_i^2 L_{m-1}\left(\xi_{mn}\right) L_{m+1}\left(\xi_{mn}\right) - r_o^2 L_{m-1}\left(\xi_{mn}\frac{r_o}{r_i}\right) L_{m+1}\left(\xi_{mn}\frac{r_o}{r_i}\right)\right]}} D_{mn} \\
&= \sqrt{\frac{(2-\delta_{m,0})}{\pi\left[r_i^2 L_{m-1}\left(\xi_{mn}\right) L_{m+1}\left(\xi_{mn}\right) - r_o^2 L_{m-1}\left(\xi_{mn}\frac{r_o}{r_i}\right) L_{m+1}\left(\xi_{mn}\frac{r_o}{r_i}\right)\right]}} D_{mn}
\end{aligned}
\tag{C.24}
$$

In Eq.C.21 we have introduced the normalization constant D_{mn}, which will be determined during the normalization procedure of the modal fields later on. We could now express the final orthogonalized

eigenfunction $\phi_{mn}(\rho,\varphi)$ as follows:

$$\phi_{mn}(\rho,\varphi)=D_{mn}\sqrt{\frac{(2-\delta_{m,0})}{\pi\left[r_i^2L_{m-1}\left(\xi_{mn}\right)L_{m+1}\left(\xi_{mn}\right)-r_o^2L_{m-1}\left(\xi_{mn}\frac{r_o}{r_i}\right)L_{m+1}\left(\xi_{mn}\frac{r_o}{r_i}\right)\right]}}\cos\left(m\varphi\right)L_m\left(\xi_{mn}\frac{\rho}{r_i}\right) \tag{C.25}$$

The transversal electric and magnetic field expansion functions $\mathbf{e}^{\mathrm{D}}_{mn}(\boldsymbol{\rho})=\mathbf{e}^{\mathrm{D}}_{mn}(\rho,\varphi)$ and $\mathbf{h}^{\mathrm{D}}_{mn}(\boldsymbol{\rho})=\mathbf{h}^{\mathrm{D}}_{mn}(\rho,\varphi)$ could now be expressed as follows:

$$\begin{aligned}
\mathbf{e}^{\mathrm{D}}_{mn}(\boldsymbol{\rho}) &= \nabla_t\phi_{mn}(\boldsymbol{\rho})\\
&= \left(\frac{\partial}{\partial\rho}\hat{\boldsymbol{\rho}}+\frac{1}{\rho}\frac{\partial}{\partial\varphi}\hat{\boldsymbol{\varphi}}\right)\phi_{mn}(\boldsymbol{\rho})\\
&= \hat{\boldsymbol{\rho}}\mathbf{e}^{\mathrm{D}}_{\rho mn}(\boldsymbol{\rho})+\hat{\boldsymbol{\varphi}}\mathbf{e}^{\mathrm{D}}_{\varphi mn}(\boldsymbol{\rho})\\
&= \hat{\boldsymbol{\rho}}D_{mn}\frac{\xi_{mn}}{r_i}\sqrt{\frac{(2-\delta_{m,0})}{\pi}}\frac{L'_m\left(\xi_{mn}\frac{\rho}{r_i}\right)}{\sqrt{\left[r_i^2L_{m-1}\left(\xi_{mn}\right)L_{m+1}\left(\xi_{mn}\right)-r_o^2L_{m-1}\left(\xi_{mn}\frac{r_o}{r_i}\right)L_{m+1}\left(\xi_{mn}\frac{r_o}{r_i}\right)\right]}}\cos\left(m\varphi\right)\\
&\quad-\hat{\boldsymbol{\varphi}}D_{mn}\frac{m}{\rho}\sqrt{\frac{(2-\delta_{m,0})}{\pi}}\frac{L_m\left(\xi_{mn}\frac{\rho}{r_i}\right)}{\sqrt{\left[r_i^2L_{m-1}\left(\xi_{mn}\right)L_{m+1}\left(\xi_{mn}\right)-r_o^2L_{m-1}\left(\xi_{mn}\frac{r_o}{r_i}\right)L_{m+1}\left(\xi_{mn}\frac{r_o}{r_i}\right)\right]}}\sin\left(m\varphi\right)\\
&= \hat{\boldsymbol{\rho}}D_{mn}\frac{\xi_{mn}}{r_i}\sqrt{\frac{(2-\delta_{m,0})}{\pi}}\frac{\left[\left(\frac{mr_i}{\xi_{mn}\rho}\right)L_m\left(\xi_{mn}\frac{\rho}{r_i}\right)-L_{m+1}\left(\xi_{mn}\frac{\rho}{r_i}\right)\right]}{\sqrt{\left[r_i^2L_{m-1}\left(\xi_{mn}\right)L_{m+1}\left(\xi_{mn}\right)-r_o^2L_{m-1}\left(\xi_{mn}\frac{r_o}{r_i}\right)L_{m+1}\left(\xi_{mn}\frac{r_o}{r_i}\right)\right]}}\cos\left(m\varphi\right)\\
&\quad-\hat{\boldsymbol{\varphi}}D_{mn}\frac{m}{\rho}\sqrt{\frac{(2-\delta_{m,0})}{\pi}}\frac{L_m\left(\xi_{mn}\frac{\rho}{r_i}\right)}{\sqrt{\left[r_i^2L_{m-1}\left(\xi_{mn}\right)L_{m+1}\left(\xi_{mn}\right)-r_o^2L_{m-1}\left(\xi_{mn}\frac{r_o}{r_i}\right)L_{m+1}\left(\xi_{mn}\frac{r_o}{r_i}\right)\right]}}\sin\left(m\varphi\right)
\end{aligned} \tag{C.26}$$

$$
\begin{aligned}
\mathbf{h}^{\mathrm{D}}_{mn}(\boldsymbol{\rho}) &= \hat{\mathbf{z}} \times \nabla_t \phi_{mn}(\boldsymbol{\rho}) \\
&= \left(\frac{\partial}{\partial \rho} \hat{\boldsymbol{\varphi}} - \frac{1}{\rho} \frac{\partial}{\partial \varphi} \hat{\boldsymbol{\rho}} \right) \phi_{mn}(\boldsymbol{\rho}) \\
&= \hat{\boldsymbol{\varphi}} \mathbf{e}^{\mathrm{D}}_{\rho mn}(\boldsymbol{\rho}) - \hat{\boldsymbol{\rho}} \mathbf{e}^{\mathrm{D}}_{\varphi mn}(\boldsymbol{\rho}) \\
&= \hat{\boldsymbol{\rho}} D_{mn} \frac{m}{\rho} \sqrt{\frac{(2-\delta_{m,0})}{\pi}} \frac{L_m\left(\xi_{mn}\frac{\rho}{r_i}\right)}{\sqrt{\left[r_i^2 L_{m-1}\left(\xi_{mn}\right) L_{m+1}\left(\xi_{mn}\right) - r_o^2 L_{m-1}\left(\xi_{mn}\frac{r_o}{r_i}\right) L_{m+1}\left(\xi_{mn}\frac{r_o}{r_i}\right)\right]}} \sin\left(m\varphi\right) \\
&\quad + \hat{\boldsymbol{\varphi}} D_{mn} \frac{\xi_{mn}}{r_i} \sqrt{\frac{(2-\delta_{m,0})}{\pi}} \frac{L'_m\left(\xi_{mn}\frac{\rho}{r_i}\right)}{\sqrt{\left[r_i^2 L_{m-1}\left(\xi_{mn}\right) L_{m+1}\left(\xi_{mn}\right) - r_o^2 L_{m-1}\left(\xi_{mn}\frac{r_o}{r_i}\right) L_{m+1}\left(\xi_{mn}\frac{r_o}{r_i}\right)\right]}} \cos\left(m\varphi\right) \\
&= \hat{\boldsymbol{\rho}} D_{mn} \frac{m}{\rho} \sqrt{\frac{(2-\delta_{m,0})}{\pi}} \frac{L_m\left(\xi_{mn}\frac{\rho}{r_i}\right)}{\sqrt{\left[r_i^2 L_{m-1}\left(\xi_{mn}\right) L_{m+1}\left(\xi_{mn}\right) - r_o^2 L_{m-1}\left(\xi_{mn}\frac{r_o}{r_i}\right) L_{m+1}\left(\xi_{mn}\frac{r_o}{r_i}\right)\right]}} \sin\left(m\varphi\right) \\
&\quad + \hat{\boldsymbol{\varphi}} D_{mn} \frac{\xi_{mn}}{r_i} \sqrt{\frac{(2-\delta_{m,0})}{\pi}} \frac{\left[\left(\frac{mr_i}{\xi_{mn}\rho}\right) L_m\left(\xi_{mn}\frac{\rho}{r_i}\right) - L_{m+1}\left(\xi_{mn}\frac{\rho}{r_i}\right)\right]}{\sqrt{\left[r_i^2 L_{m-1}\left(\xi_{mn}\right) L_{m+1}\left(\xi_{mn}\right) - r_o^2 L_{m-1}\left(\xi_{mn}\frac{r_o}{r_i}\right) L_{m+1}\left(\xi_{mn}\frac{r_o}{r_i}\right)\right]}} \cos\left(m\varphi\right)
\end{aligned}
\tag{C.27}
$$

Continuing forward, we will denote $i = mn$ as a collective term for variable parameters, which is introduced for convenience. We could now obtain the unnormalized TM field expressions by appending the following excitation functions $u_i^{\mathrm{D}}(z,t)$, $i_i^{\mathrm{D}}(z,t)$, and $l_i^{\mathrm{D}}(z,t)$ and sum over all the excited modes as follows:

$$
\begin{aligned}
\mathbf{E}(\mathbf{r},t) &= \mathbf{E}_t(\mathbf{r},t) + \mathbf{E}_z(\mathbf{r},t) \\
&= \sum_{i=1}^{\infty} u_i^{\mathrm{D}}(z,t) \mathbf{e}_i^{\mathrm{D}}(\boldsymbol{\rho}) + \sum_{i=1}^{\infty} l_i^{\mathrm{D}}(z,t) \phi_i(\boldsymbol{\rho}) \hat{\mathbf{z}}
\end{aligned}
\tag{C.28}
$$

$$
\mathbf{H}_t(\mathbf{r},t) = \sum_{i=1}^{\infty} i_i^{\mathrm{D}}(z,t) \mathbf{h}_i^{\mathrm{D}}(\boldsymbol{\rho})
\tag{C.29}
$$

We proceed by expressing the source-free free-space TM excitation problem in both the time and frequency domain, where the conversion between the two domains has been achieved using the $j\omega$-method:

Time-domain formulation:

$$
\left.
\begin{aligned}
&\frac{\partial u_i^{\mathrm{D}}(z,t)}{\partial z} + \mu_0 \frac{\partial i_i^{\mathrm{D}}(z,t)}{\partial t} - l_i^{\mathrm{D}}(z,t) = 0 \\
&i_i^{\mathrm{D}}(z,t) + \frac{\varepsilon_0}{d_{ti}^2} \frac{\partial l_i^{\mathrm{D}}(z,t)}{\partial t} = 0 \\
&\frac{\partial i_i^{\mathrm{D}}(z,t)}{\partial z} + \varepsilon_0 \frac{\partial u_i^{\mathrm{D}}(z,t)}{\partial t} = 0
\end{aligned}
\right\}
\tag{C.30}
$$

Frequency-domain formulation:

$$
\left.
\begin{aligned}
&\frac{\partial U_i^{\mathrm{D}}(z,\omega)}{\partial z} + j\omega\mu_0 I_i^{\mathrm{D}}(z,\omega) - L_i^{\mathrm{D}}(z,\omega) = 0 \\
&I_i^{\mathrm{D}}(z,\omega) + j\omega \frac{\varepsilon_0}{d_{ti}^2} L_i^{\mathrm{D}}(z,\omega) = 0 \\
&\frac{\partial I_i^{\mathrm{D}}(z,\omega)}{\partial z} + j\omega\varepsilon_0 U_i^{\mathrm{D}}(z,\omega) = 0
\end{aligned}
\right\}
\tag{C.31}
$$

For simplicity, we assume one operating frequency and proceed with solving the frequency-domain formulation as a system of equations:

$$\left.\begin{aligned} &\frac{\partial^2 U_i^{\mathrm{D}}(z)}{\partial z^2} + d_{zi}^2 U_i^{\mathrm{D}}(z) = 0 \\ &\frac{\partial U_i^{\mathrm{D}}(z)}{\partial z} + j\frac{\eta d_{zi}^2}{k} I_i^{\mathrm{D}}(z) = 0 \\ &I_i^{\mathrm{D}}(z) + j\omega\frac{\varepsilon_0}{d_{ti}^2} L_i^{\mathrm{D}}(z) = 0 \end{aligned}\right\} \tag{C.32}$$

The aforementioned system of equations yields the following solution for each excitation function:

$$\left.\begin{aligned} U_i^{\mathrm{D}}(z) &= a_i^{\mathrm{D}+} e^{-jd_{zi}z} + a_i^{\mathrm{D}-} e^{+jd_{zi}z} \\ I_i^{\mathrm{D}}(z) &= \frac{k}{\eta d_{zi}} \left(a_i^{\mathrm{D}+} e^{-jd_{zi}z} - a_i^{\mathrm{D}-} e^{+jd_{zi}z}\right) \\ L_i^{\mathrm{D}}(z) &= \frac{jd_{ti}^2}{d_{zi}} \left(a_i^{\mathrm{D}+} e^{-jd_{zi}z} - a_i^{\mathrm{D}-} e^{+jd_{zi}z}\right) \end{aligned}\right\} \tag{C.33}$$

Here we have introduced the free-space wave number $k = \omega^2\mu_0\varepsilon_0$, the free-space wave impedance $\eta = \sqrt{\mu_0/\varepsilon_0}$, the longitudinal eigenvalue $d_{zi} = \sqrt{k^2 - d_{ti}^2}$ where $\mathrm{Im}\{d_{zi}\} < 0$, and the undetermined excitation coefficients $a_i^{\mathrm{D}\pm}$. The normalized TM field expression is now obtained as follows:

$$\boldsymbol{E}^{\mathrm{TM}}(\mathbf{r}) = \sum_{i=1}^{\infty} \left[a_i^{\mathrm{D}+} e^{-jd_{zi}z} \boldsymbol{E}_i^{\mathrm{D}+}(\boldsymbol{\rho}) + a_i^{\mathrm{D}-} e^{+jd_{zi}z} \boldsymbol{E}_i^{\mathrm{D}-}(\boldsymbol{\rho})\right] \tag{C.34}$$

$$\boldsymbol{H}^{\mathrm{TM}}(\mathbf{r}) = \sum_{i=1}^{\infty} \left[a_i^{\mathrm{D}+} e^{-jd_{zi}z} \boldsymbol{H}_i^{\mathrm{D}+}(\boldsymbol{\rho}) + a_i^{\mathrm{D}-} e^{+jd_{zi}z} \boldsymbol{H}_i^{\mathrm{D}-}(\boldsymbol{\rho})\right] \tag{C.35}$$

Where the modal fields are re-expressed as follows:

$$\boldsymbol{E}_i^{\mathrm{D}\pm}(\boldsymbol{\rho}) = \boldsymbol{e}_i^{\mathrm{D}}(\boldsymbol{\rho}) \pm \frac{jd_{ti}^2}{d_{zi}} \phi_i(\boldsymbol{\rho})\hat{\mathbf{z}} \tag{C.36}$$

$$\boldsymbol{H}_i^{\mathrm{D}\pm}(\boldsymbol{\rho}) = \pm\frac{k}{\eta d_{zi}} \boldsymbol{h}_i^{\mathrm{D}}(\boldsymbol{\rho}) \tag{C.37}$$

As a normalization condition, we require the modal fields to transport one unit of apparent power along the waveguide cross-section:

$$\begin{aligned} \left|\frac{1}{2}\int_A \left(\boldsymbol{E}_i^{\mathrm{D}\pm} \times \boldsymbol{H}_i^{\mathrm{D}\pm}\right) \cdot \hat{\mathbf{z}} ds\right| &= \left|\frac{1}{2}\int_0^{2\pi}\int_{r_i}^{r_o} \left(\boldsymbol{E}_i^{\mathrm{D}\pm} \times \boldsymbol{H}_i^{\mathrm{D}\pm}\right) \cdot \hat{\mathbf{z}} \rho d\rho d\varphi\right| \\ &= \left|\frac{1}{2}\int_0^{2\pi}\int_{r_i}^{r_o} \left(\left[\boldsymbol{e}_i^{\mathrm{D}}(\boldsymbol{\rho}) \pm \frac{jd_{ti}^2}{d_{zi}}\phi_i(\boldsymbol{\rho})\hat{\mathbf{z}}\right] \times \pm\frac{k}{\eta d_{zi}} \boldsymbol{h}_i^{\mathrm{D}}(\boldsymbol{\rho})\right) \cdot \hat{\mathbf{z}} \rho d\rho d\varphi\right| \\ &= \left|\frac{1}{2}\int_0^{2\pi}\int_{r_i}^{r_o} \left(\boldsymbol{e}_i^{\mathrm{D}}(\boldsymbol{\rho}) \times \frac{k}{\eta d_{zi}} \boldsymbol{h}_i^{\mathrm{D}}(\boldsymbol{\rho})\right) \cdot \hat{\mathbf{z}} \rho d\rho d\varphi\right| \\ &= \left|\frac{k}{2\eta d_{zi}}\int_0^{2\pi}\int_{r_i}^{r_o} \left(\boldsymbol{e}_i^{\mathrm{D}}(\boldsymbol{\rho}) \times \boldsymbol{h}_i^{\mathrm{D}}(\boldsymbol{\rho})\right) \cdot \hat{\mathbf{z}} \rho d\rho d\varphi\right| \\ &= \left|\frac{k}{2\eta d_{zi}} d_{ti}^2 D_i^2\right| \\ &= 1 \end{aligned} \tag{C.38}$$

Here we have exploited the inherited orthogonality relation for the transversal field expansion functions, which is presented in Eq.5.67a from the Compendium. The normalization constant D_i could now be defined as follows:

$$D_i = \frac{1}{d_{ti}}\sqrt{\frac{2\eta\,|d_{zi}|}{k}} \tag{C.39}$$

By re-introducing the collective term $i = mn$, the power normalized modal field could now be explicitly expressed as follows:

$$\begin{aligned}
\boldsymbol{E}^{\mathrm{D}\pm}_{mn}(\boldsymbol{\rho}) &= \boldsymbol{e}^{\mathrm{D}}_{mn}(\boldsymbol{\rho}) \pm \frac{jd^2_{tmn}}{d_{zmn}}\phi_{mn}(\boldsymbol{\rho})\hat{\mathbf{z}} \\
&= \hat{\boldsymbol{\rho}}\frac{\xi_{mn}}{d_{tmn}r_i}\sqrt{\frac{2\eta\left|d_{zmn}\right|(2-\delta_{m,0})}{k\pi}}\frac{\left[\left(\frac{mr_i}{\xi_{mn}\rho}\right)L_m\left(\xi_{mn}\frac{\rho}{r_i}\right) - L_{m+1}\left(\xi_{mn}\frac{\rho}{r_i}\right)\right]\cos(m\varphi)}{\sqrt{\left[r_i^2 L_{m-1}(\xi_{mn})L_{m+1}(\xi_{mn}) - r_o^2 L_{m-1}\left(\xi_{mn}\frac{r_o}{r_i}\right)L_{m+1}\left(\xi_{mn}\frac{r_o}{r_i}\right)\right]}} \\
&\quad - \hat{\boldsymbol{\varphi}}\frac{m}{d_{tmn}\rho}\sqrt{\frac{2\eta\left|d_{zmn}\right|(2-\delta_{m,0})}{k\pi}}\frac{L_m\left(\xi_{mn}\frac{\rho}{r_i}\right)\sin(m\varphi)}{\sqrt{\left[r_i^2 L_{m-1}(\xi_{mn})L_{m+1}(\xi_{mn}) - r_o^2 L_{m-1}\left(\xi_{mn}\frac{r_o}{r_i}\right)L_{m+1}\left(\xi_{mn}\frac{r_o}{r_i}\right)\right]}} \\
&\quad \pm \hat{\mathbf{z}}\frac{jd_{tmn}}{d_{zmn}}\sqrt{\frac{2\eta\left|d_{zmn}\right|(2-\delta_{m,0})}{k\pi}}\frac{L_m\left(\xi_{mn}\frac{\rho}{r_i}\right)\cos(m\varphi)}{\sqrt{\left[r_i^2 L_{m-1}(\xi_{mn})L_{m+1}(\xi_{mn}) - r_o^2 L_{m-1}\left(\xi_{mn}\frac{r_o}{r_i}\right)L_{m+1}\left(\xi_{mn}\frac{r_o}{r_i}\right)\right]}}
\end{aligned} \tag{C.40}$$

$$\begin{aligned}
\boldsymbol{H}^{\mathrm{D}\pm}_{mn}(\boldsymbol{\rho}) &= \pm\frac{k}{\eta d_{zmn}}\boldsymbol{h}^{\mathrm{D}}_{mn}(\boldsymbol{\rho}) \\
&= \pm\hat{\boldsymbol{\rho}}\frac{m}{d_{tmn}d_{zmn}\rho}\sqrt{\frac{2k\left|d_{zmn}\right|(2-\delta_{m,0})}{\pi\eta}}\frac{L_m\left(\xi_{mn}\frac{\rho}{r_i}\right)\sin(m\varphi)}{\sqrt{\left[r_i^2 L_{m-1}(\xi_{mn})L_{m+1}(\xi_{mn}) - r_o^2 L_{m-1}\left(\xi_{mn}\frac{r_o}{r_i}\right)L_{m+1}\left(\xi_{mn}\frac{r_o}{r_i}\right)\right]}} \\
&\quad \pm\hat{\boldsymbol{\varphi}}\frac{\xi_{mn}}{d_{tmn}d_{zmn}r_i}\sqrt{\frac{2k\left|d_{zmn}\right|(2-\delta_{m,0})}{\pi\eta}}\frac{\left[\left(\frac{mr_i}{\xi_{mn}\rho}\right)L_m\left(\xi_{mn}\frac{\rho}{r_i}\right) - L_{m+1}\left(\xi_{mn}\frac{\rho}{r_i}\right)\right]\cos(m\varphi)}{\sqrt{\left[r_i^2 L_{m-1}(\xi_{mn})L_{m+1}(\xi_{mn}) - r_o^2 L_{m-1}\left(\xi_{mn}\frac{r_o}{r_i}\right)L_{m+1}\left(\xi_{mn}\frac{r_o}{r_i}\right)\right]}}
\end{aligned} \tag{C.41}$$

The complete power normalized frequency domain electric and magnetic field expressions could now be expressed using Eq.C.34, Eq.C.35, Eq.C.40 and Eq.C.41.